JMS

Collision-induced dissociation pathways of yeast sphingolipids and their molecular profiling in total lipid extracts: a study by quadrupole TOF and linear ion trap–orbitrap mass spectrometry

Christer S. Ejsing,[1] Thomas Moehring,[2] Ute Bahr,[3] Eva Duchoslav,[4] Michael Karas,[3] Kai Simons[1] and Andrej Shevchenko[1]*

[1] Max Planck Institute of Molecular Cell Biology and Genetics, 01307 Dresden, Germany

[2] ThermoElectron (Bremen) GmbH, 28119 Bremen, Germany

[3] Johann Wolfgang Goethe-University, 60439 Frankfurt am Main, Germany

[4] MDS Sciex, L4K 4V8 Concord, ON, Canada

The yeast *Saccharomyces cerevisiae* synthesizes three classes of sphingolipids: inositolphosphoceramides (IPCs), mannosyl-inositolphosphoceramides (MIPCs), and mannosyl-diinositolphosphoceramides (M(IP)$_2$C). Tandem mass spectrometry of their molecular anions on a hybrid quadrupole time-of-flight (QqTOF) instrument produced fragments of inositol-containing head groups, which were specific for each lipid class. MS^n analysis performed on a hybrid linear ion trap–orbitrap (LTQ Orbitrap) mass spectrometer with better than 3 ppm mass accuracy identified fragment ions specific for the amide-linked fatty acid and the long chain base moieties in individual molecular species. By selecting *m/z* of class-specific fragment ions for multiple precursor ion scanning, we profiled yeast sphingolipids in total lipid extracts on a QqTOF mass spectrometer. Thus, a combination of QqTOF and LTQ Orbitrap mass spectrometry lends itself to rapid, comprehensive and structure-specific profiling of the molecular composition of sphingolipids and glycerophospholipids in important model organisms, such as fungi and plants. Copyright © 2006 John Wiley & Sons, Ltd.
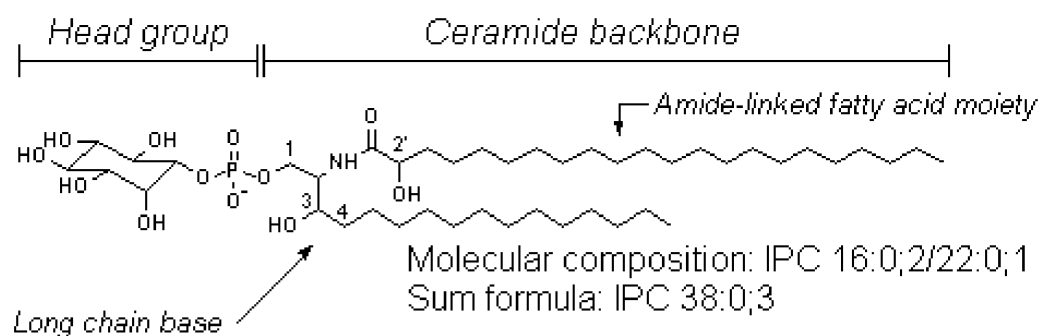
INTRODUCTION

The yeasts *Saccharomyces cerevisiae* and *Schizosaccharomyces pombe* are the recognized eukaryotic model organisms to study lipid metabolism and structural microheterogeneity of cell membranes (lipid rafts) that provide a valuable insight into the corresponding cellular machinery in higher eukaryotes, including humans.[1–4] Therefore the characterization of the yeast lipidome, complementing ongoing proteomic and functional genomic efforts, is currently receiving increased attention.

Methods for the analysis of glycerophospholipids by mass spectrometry have been developed and successfully used in lipid biochemistry in yeasts.[5] In this work, we have focused on inositol-containing yeast sphingolipids, which are

*Correspondence to: Andrej Shevchenko, MPI of Molecular Cell Biology and Genetics, Pfotenhauerstrasse 108, 01307 Dresden, Germany. E-mail: shevchenko@mpi-cbg.de

involved in numerous cellular processes, such as heat-stress response, calcium homeostasis, protein sorting, and cell surface polarization.[6–11] Wild-type *S. cerevisiae* synthesizes sphingolipids of three classes: inositolphosphoceramides (IPCs), mannosyl-inositolphosphoceramides (MIPCs), and mannosyl-diinositolphosphoceramides (M(IP)$_2$Cs),[1,6,12,13] which are enriched in the plasma membrane, where they constitute 20–30% of all lipids.[14] Inositol-containing sphingolipids consist of three structural elements: a long chain base and an amide-linked fatty acid that form the apolar ceramide backbone, to which a polar head group is attached via a phosphate moiety (Fig. 1). The structural diversity of yeast sphingolipids stems from the variability of their head groups, as well as from the number of carbon atoms and the number and position of hydroxyl groups and double bonds in their ceramide backbone.[1,15] In *S. cerevisiae*, long chain bases typically contain 16 to 20 carbon atoms and two (in dihydrosphingosines) or three (in phytosphingosines) hydroxyl groups, which, in combination with various amide-linked fatty acid moieties, give rise to sphingolipids with a dihydroceramide or phytoceramide backbone, respectively (Fig. 1).
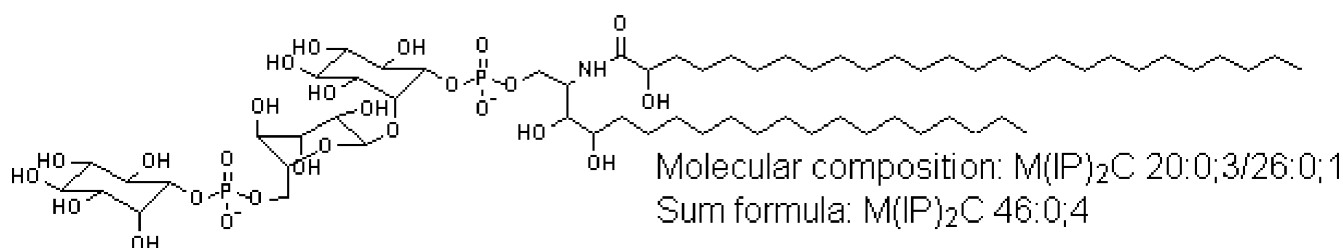
Inositolphosphoceramide (IPC):

Mannosyl-inositolphosphoceramide (MIPC):
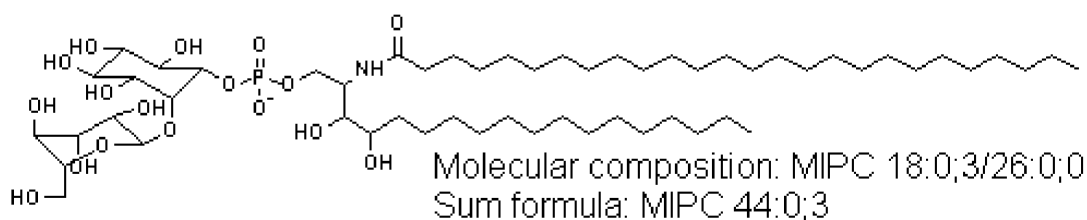
Mannosyl-diinositolphosphoceramide (M(IP)₂C):

Figure 1. Structure of yeast sphingolipids. Inositol-containing sphingolipids consist of a long chain base and an amide-linked fatty acid that together constitute a ceramide backbone, to which a polar head group is attached via a phosphate moiety. The long chain base and the fatty acid moiety typically comprise 16 to 20 and 20 to 26 carbon atoms, respectively. The long chain base might comprise two (dihydrosphingosine) or three (phytosphingosine) hydroxyl groups at positions 1, 3, and 4 that form dihydroceramides or phytoceramides, respectively. The amide-linked fatty acid moiety can be non-, mono-, or dihydroxylated, with one hydroxyl group at position 2' (α-hydroxyl group) and the other groups elsewhere between positions 9' and 16'. In this work, yeast sphingolipids were annotated either by their molecular composition or by the sum formula. The molecular composition indicates the number of carbon atoms, double bonds, and hydroxyl groups separately in the long chain base and in the fatty acid moiety, whereas the sum formula provides the total number of carbon atoms, double bonds, and hydroxyl groups in the entire ceramide backbone. The species annotation convention is explained in the 'Experimental' section.

The amide-linked fatty acid moiety is typically composed of 26 carbon atoms and could be mono- or dihydroxylated or contain no hydroxyl groups.

Chemical derivatization,[16] gas chromatography–mass spectrometry (GC–MS)[17] and magnetic sector mass spectrometry[18] revealed that within each class yeast sphingolipids are diverse. However, detailed characterization of their profiles proved difficult because the available analytical approaches were laborious and offered low sensitivity.

Electrospray ionization mass spectrometry enables the identification and quantification of lipid species in minute amounts of total lipid extracts.[19–21] Lipid classes can be either preseparated by high-performance liquid chromatography interfaced on line to a mass spectrometer,[22] or alternatively, unseparated lipid extracts can be directly infused into a mass spectrometer using a conventional or a nanoelectrospray ion source.[23] Direct mass spectrometric profiling is typically performed in precursor ion scanning mode, which relies on the detection of the characteristic fragment ion produced from molecular ions of lipids of a given class upon their collision-induced dissociation in a tandem mass spectrometer.[5,23] Triple quadrupole mass spectrometers can only acquire one precursor ion scan spectrum at a time, whereas multiple precursor ion scans can be simultaneously acquired by a hybrid quadrupole time-of-flight (QqTOF 'q'

stands for RF-only quadrupole of the collision cell) mass spectrometer.[24,25] Multiple precursor ion scanning enhances the specificity and throughput of lipid profiling without compromising the sensitivity, compared to conventional triple quadrupole machines.

We used QqTOF[26] and linear ion trap–orbitrap (LTQ Orbitrap)[27,28] mass spectrometers to elucidate fragmentation pathways of yeast inositol-containing sphingolipids and identified fragment ions that either were specific for each lipid class or characterized the ceramide backbone in individual lipid species. Subsequent QqTOF analysis using the method of multiple precursor ion scanning, based on m/z of class-specific fragments, enabled simultaneous profiling of sphingolipids and glycerophospholipids in total yeast lipid extracts.

EXPERIMENTAL

Chemicals, cell media, and lipid standards

All common chemicals were purchased from Sigma Chemicals (St. Louis, MO) and were of analytical grade. The solvents water, methanol (both LiChrosolv® grade), chloroform (LC grade), acetic acid, and 25% ammonia solution (reagent grade) were from Merck (Darmstadt, Germany). Yeast extract, peptone, and dextrose were purchased from Difco Laboratories (BD GmbH, Heidelberg, Germany). 1-Palmitoyl-2-docosahexaenoyl-*sn*-glycero-3-phosphocholine was purchased from Avanti Polar Lipids, Inc. (Alabaster, AL).

Yeast strains and growth conditions

Yeast strains used in this study were *S. cerevisiae* RH690-15D (wild type); mutant strains *elo3Δ*, *sur2Δ*, and *scs7Δ* produced in the BY4741 background, obtained from Euroscarf (Frankfurt am Main, Germany); the double null mutant *scs7Δ sur2Δ* kindly provided by Dr Teresa Dunn; *S. pombe* strain FY254 and *Pichia pastoris* strain SmdII 684. Yeast cells were grown at 30 °C to log phase in rich medium (yeast extract/peptone/dextrose), prepared as previously described.[29]

Lipid extraction and alkaline hydrolysis

Yeasts were harvested by centrifugation for 5 min at 1000 g, and washed twice in a cold lysis buffer (25 mM Tris, 5 mM EDTA, pH 8.5). Pelleted yeast was stored at −80 °C. Upon thawing, the pellet was resuspended in a cold lysis buffer to a density of 4 OD600 unit/ml. Cells were lysed by vortexing their suspension with glass beads for 5 min at 4 °C.[30] The cell lysate was then cleared of glass beads by centrifugation for 5 min at 500 g and 4 °C.

The cell lysate was mixed with chloroform/methanol/water/pyridine (60:30:6:1) and extracted at 60 °C for 2 h.[31] The extract was dried in a vacuum centrifuge, followed by either mild alkaline hydrolysis or resuspension in chloroform/methanol/water (16:16:5) and stored at −20 °C.

To hydrolyze glycerophospholipids, the extracted cell lysate was dissolved in methanol containing 0.1 M NaOH and vortexed at 30 °C for 2 h.[16,18] 1 M acetic acid and 0.5% (w/w) ethylenediaminetetraacetic acid (EDTA) were

added to adjust the pH of the reaction mixture to be neutral. Chloroform was added to induce phase separation and the organic phase was recovered and evaporated to dryness in a vacuum centrifuge. Extracted sphingolipids were redissolved in chloroform/methanol/water (16:16:5) and stored at −20 °C.

Fractionation of sphingolipids by TLC

Preparative thin-layer chromatography (TLC) was carried out on aluminium-back silica 60 high-performance plates (Camag, Muttenz, Switzerland) essentially, as described by Hechtberger *et al.*[18] A total lipid extract dissolved in chloroform/methanol/water (16:16:5) was loaded as a 5-cm lane in the center of a silica plate and developed in chloroform/methanol/4.2 M ammonia (9:7:2) or chloroform/methanol/acetic acid/water (16:6:4:1.6). The developed silica plates were dried and cut in half, and one-half was subjected to sulfuric acid staining. Subsequently, the two parts were aligned, and strips containing M(IP)₂C, MIPC, and IPC sphingolipids were excised from an unstained part of the TLC plate. Silica strips were extracted with chloroform/methanol/water (16:16:5) for 1 h by vortexing, and sphingolipid class fractions thus obtained were stored at −20 °C.

Quadrupole time-of-flight mass spectrometry

Mass spectrometric analysis was performed in negative ion mode on a modified QSTAR Pulsar *i* QqTOF mass spectrometer (MDS Sciex, Concord, Canada) equipped with an automated nanoflow ion source NanoMate HD System (Advion BioSciences Ltd, Ithaca, NJ). Ionization voltage was set to 1.05 kV, gas pressure to 0.1 psi, and the source was controlled by Chipsoft 6.3.2 software from the same company. The instrument was calibrated in MS/MS mode using a synthetic lipid standard, 1-palmitoyl-2-docosahexaenoyl-*sn*-glycero-3-phosphocholine as described previously.[32]

Prior to the analysis, a methanol solution of ammonium acetate was added to lipid extracts to a final concentration of 5 mM. Tandem mass spectra were acquired at the collision energy offset in the range of 25 to 85 eV and the analytical quadrupole Q1 was operated at the low mass resolution settings that enabled unperturbed transmission of entire isotopic clusters. Multiple precursor ion scanning was performed as described previously.[24] Analytical quadrupole Q1 was operated at the unit mass resolution settings at 20 ms dwell time with a step size of 0.2 Th. The selected fragment ions were listed separately for every experiment described. Peak enhancement (trapping of fragment ions within the selected range of m/z in the collision cell)[33] was applied according to the instructions of the manufacturer and controlled by Analyst QS 1.1 software. Multiple precursor ion scanning spectra were interpreted using the prototype *Lipid Profiler* software (MDS Sciex, Concord, Canada).

Mass spectrometry on ion trap and hybrid LTQ Orbitrap instruments

MS^n fragmentation was performed on a quadrupole ion trap mass spectrometer LCQ (ThermoElectron Corp., San Jose,
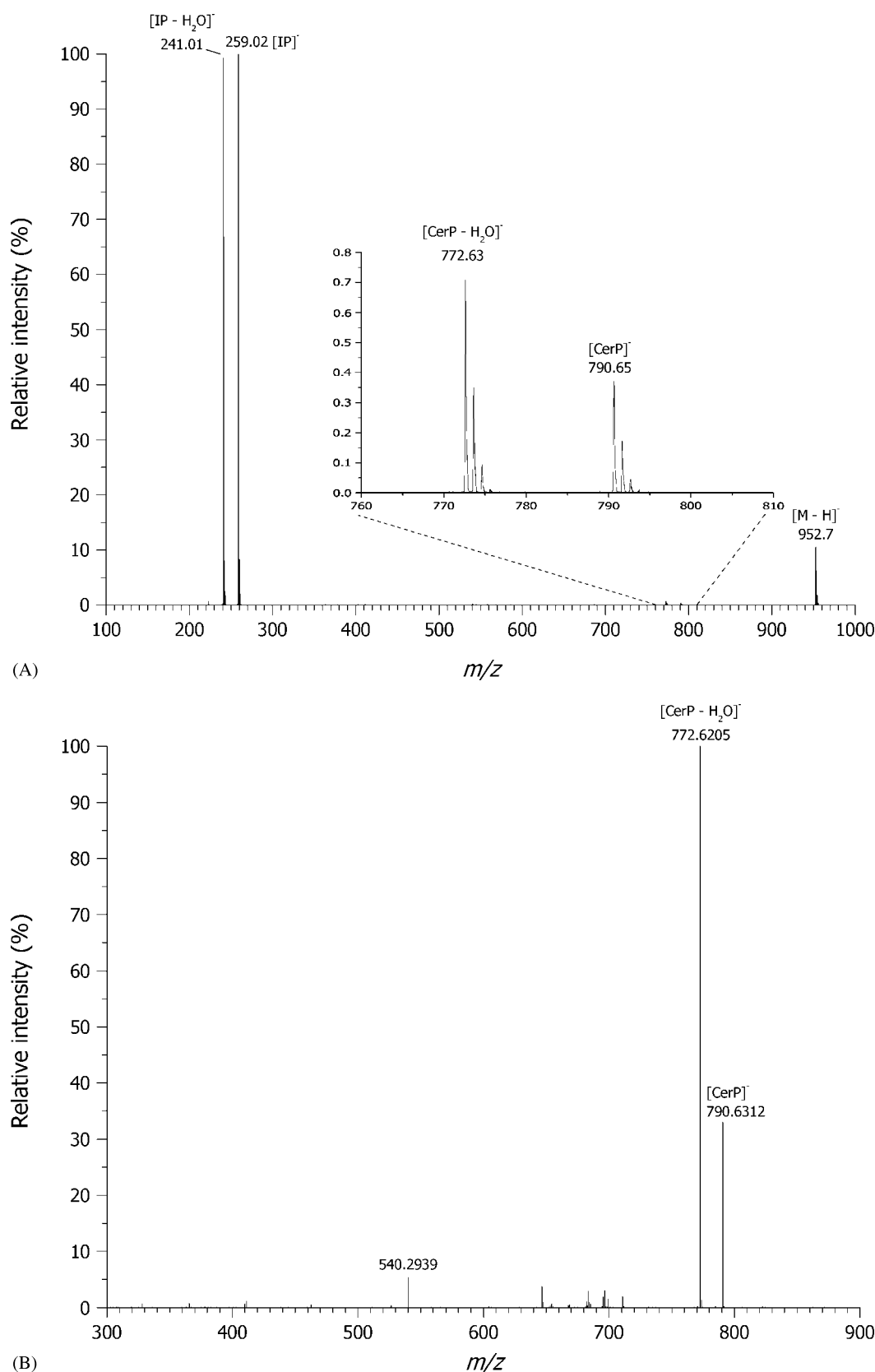
Figure 2. Fragmentation pathways of IPC species. (A) QqTOF MS/MS spectrum of IPC 44:0;4 ion of m/z 952.7 ([M – H]$^-$) acquired at the collision energy of 68 eV. (B) Orbitrap MS^2 spectrum acquired from the same precursor. (C) Orbitrap MS^3 spectrum acquired from the precursor ion m/z 772.6205 ([CerP – H$_2$O]$^-$) at the relative collision energy of 24%. Peaks with m/z 462.6826, 409.8589, 365.5548, and 296.0985 originated from the background and were not detectable in the corresponding ion trap MS^3 spectrum (data not shown). (D) Major fragmentation pathways of IPC 18:0;3/26:0;1 elucidated by QqTOF MS/MS and LTQ Orbitrap MS^n analysis. The structure of the [CerP – H$_2$O]$^-$ fragment ion with m/z 772.6225 is presented with a cyclic phosphate residue between the hydroxyl groups at positions 1 and 3 of the long chain moiety; however, isomer structures are possible.
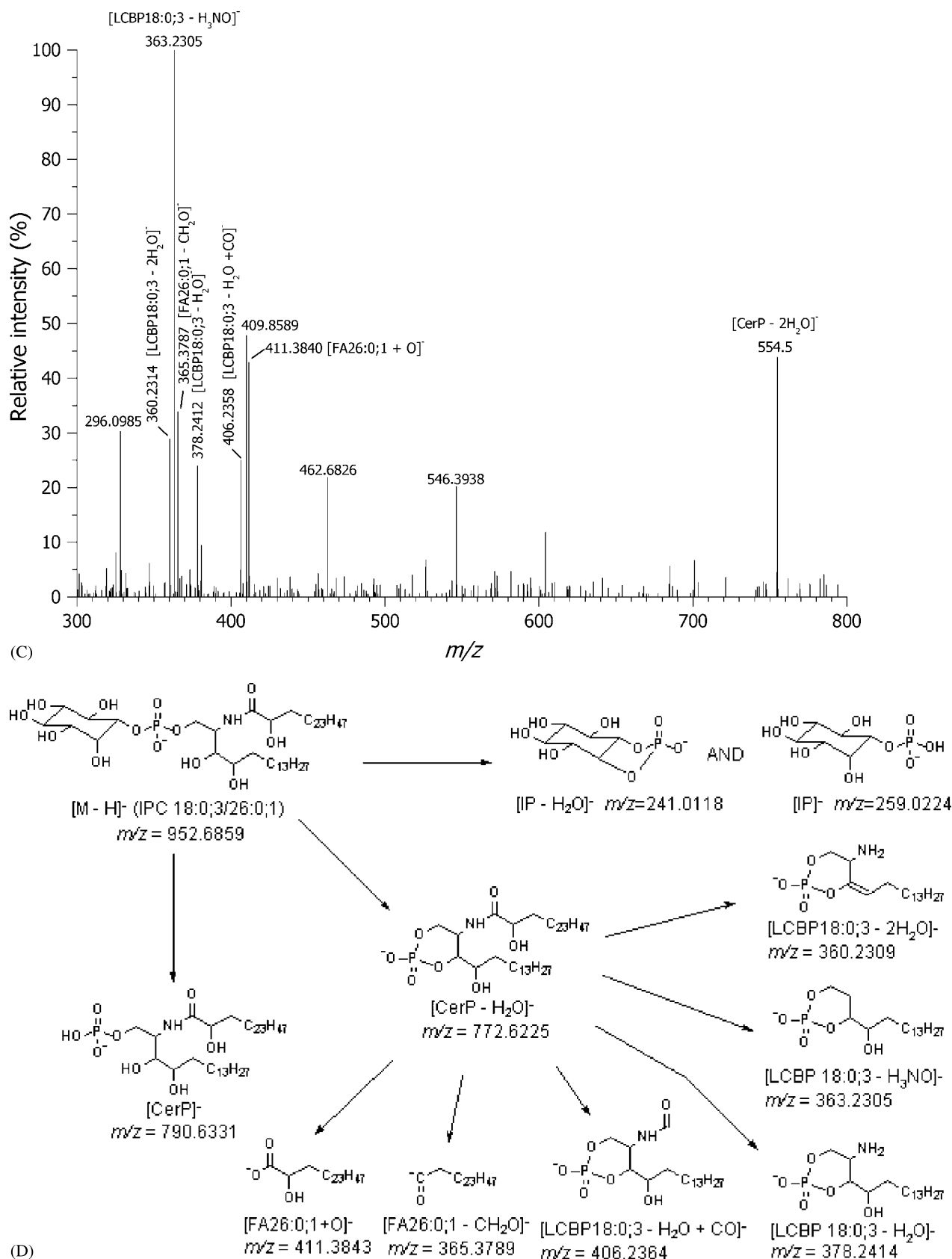
(C) spectrum plot, Relative intensity (%) vs *m/z*

Peaks labeled:
- 296.0985
- 360.2314 [LCBP18:0;3 - 2H$_2$O]$^-$
- 363.2305 [LCBP18:0;3 - H$_3$NO]$^-$ (100%)
- 365.3787 [FA26:0;1 - CH$_2$O]$^-$
- 378.2412 [LCBP18:0;3 - H$_2$O]$^-$
- 406.2358 [LCBP18:0;3 - H$_2$O +CO]$^-$
- 409.8589
- 411.3840 [FA26:0;1 + O]$^-$
- 462.6826
- 546.3938
- 554.5 [CerP - 2H$_2$O]$^-$

(D) Fragmentation scheme:

[M - H]$^-$ (IPC 18:0;3/26:0;1) *m/z* = 952.6859

[IP - H$_2$O]$^-$ *m/z* = 241.0118   AND   [IP]$^-$ *m/z* = 259.0224

[CerP - H$_2$O]$^-$ *m/z* = 772.6225

[CerP]$^-$ *m/z* = 790.6331

[LCBP18:0;3 - 2H$_2$O]$^-$ *m/z* = 360.2309

[LCBP 18:0;3 - H$_3$NO]$^-$ *m/z* = 363.2305

[FA26:0;1+O]$^-$ *m/z* = 411.3843

[FA26:0;1 - CH$_2$O]$^-$ *m/z* = 365.3789

[LCBP18:0;3 - H$_2$O + CO]$^-$ *m/z* = 406.2364

[LCBP 18:0;3 - H$_2$O]$^-$ *m/z* = 378.2414

Figure 2. (*Continued*).

CA) as previously described,[25] and LTQ Orbitrap[27,28] from the same company equipped with the NanoMate HD ion source (Advion BioSciences Ltd, Ithaca, NJ). MS analysis was performed in negative ion mode. The instrument was calibrated externally according to the instructions of the manufacturer. MS[2] and MS[3] spectra were acquired under operator control with the target mass resolution of $R = 30\,000$ at *m/z* 400 (Full Width at Half-Maximum, FWHM) and

the acquisition time period of 0.5 s/scan. The normalized collision energies of 20% and 26% were applied in MS^2 and MS^3 experiments, respectively. The activation time was set at 30 ms with the activation parameter $q = 0.25$. For MS^2 and MS^3 analysis, precursor ions were isolated within the range of 3 and 5 Th, respectively. The mass accuracy was better than 3 ppm for MS and MS^n experiments.

Annotation of lipid species and their fragment ions

Yeast sphingolipid species were annotated either by their molecular composition or by the sum formula, depending on the method of their structural characterization (Fig. 1). To denote the molecular composition the following convention was applied: <Lipid class><Number of carbon atoms in the long chain base moiety>:<Number of double bonds in the long chain base moiety>;<Number of hydroxyl groups in the long chain base moiety>/<Number of carbon atoms in the fatty acid moiety>:<Number of double bonds in the fatty acid moiety>;<Number of hydroxyl groups in the fatty acid moiety>. For example, a peak at m/z 952.7 was identified as IPC 18:0;3/26:0;1 (Fig. 2), i.e. as an IPC whose long chain base consisted of C18 phytosphingosine with no double bonds and three hydroxyl groups. Its amide-linked fatty acid moiety comprised 26 carbon atoms, no double bonds and one hydroxyl group. If the composition of the fatty acid moiety and long chain base were not separately determined, sphingolipids were characterized by the sum formula of their ceramide backbone:<Lipid class><Number of carbon atoms in the ceramide backbone>:<Number of double bonds in the ceramide backbone>;<Number of hydroxyl groups in the ceramide backbone>. For example, a peak detected at m/z 938.7 (Table 2) was identified as IPC 42:1;5, i.e. as an IPC containing a total of 42 carbon atoms, one double bond, and five hydroxyl groups in its entire ceramide backbone.

Glycerophospholipids were denoted by their molecular composition as follows: <Lipid class><Number of carbon atoms in the first fatty acid moiety>:<Number of double bonds in the first fatty acid moiety>-<Number of carbon atoms in the second fatty acid moiety>:<Number of double bonds in the second fatty acid moiety>. This notation did not, however, indicate the exact position of fatty acid moieties (sn-1 or sn-2) at the glycerol backbone. Phosphatidic acid, phosphatidylserine, phosphatidylethanolamine, phosphatidylcholine, and phosphatidylinositol species were designated as PA, PS, PE, PC, and PI, respectively. For example, a peak detected at m/z 714.6 (Fig. 6) was identified as PE 16:1–18:1, i.e. a phosphatidylethanolamine comprising the moieties of the C16 fatty acid with one double bond and the C18 fatty acid with one double bond.

Fragment ions corresponding to long chain base phosphate, ceramide, ceramide phosphate and fatty acid moieties of the analyzed lipids are designated as LCBP, Cer, CerP, and FA, respectively.

Fragment ions produced by neutral loss of inositol and phosphate are designated as -I; and -P; respectively.

RESULTS AND DISCUSSION

To elucidate the fragmentation pathways of the three inositol-containing sphingolipid classes – IPC, MIPC, and $M(IP)_2C$,

we isolated them by preparative TLC from the lipid extracts of wild-type *S. cerevisiae*[18] and from three null mutants (i.e. *scs7Δ*, *sur2Δ* and *scs7Δsur2Δ*), which are known to synthesize sphingolipids having altered structures of their ceramide backbones. Individual species within the same lipid class were subjected to tandem mass spectrometry on the QSTAR and LTQ Orbitrap mass spectrometers, whereby fragment ions that were either specific for a head group (and hence to a given lipid class) or for a ceramide backbone of individual species were identified.

Fragmentation pathways of IPCs

The most abundant ions in the IPC fraction isolated from wild-type strain of *S. cerevisiae* were detected at m/z 952.70, 968.70, and 980.73, corresponding to IPC 44:0;4, IPC 44:0;5, and IPC 46:0;4, respectively (data not shown), as was previously observed.[18,34] Tandem mass spectra of all species acquired on a QqTOF instrument were dominated by two fragment ions at m/z 259.02 ($[IP]^-$) and 241.01 ($[IP – H_2O]^-$), both originating from the inositolphosphate head group (Fig. 2(A,D)). These fragments are also typical for tandem mass spectra of phosphatidylinositols.[35] Since m/z of IPC species do not overlap with m/z of phosphatidylinositols that comprise common fatty acid moieties, the fragment ion with m/z 241.0 was previously used for profiling IPC species by precursor ion scanning.[36] Two fragment ions of very low abundance, detected at m/z 790.65 and 772.63, were produced via neutral loss of the head group as dehydroinositol ($\Delta m = 162.05$ Th) followed by the loss of H_2O, corresponding to the two ceramide phosphate fragments $[CerP]^-$ and $[CerP – H_2O]^-$, respectively (Fig. 2(D)). Efficient fragmentation of IPCs was achieved at the collision energy offset of 65–75 eV, compared to the 40–55 eV that was typically required for the fragmentation of glycerophospholipids.[25] Although the ratio of intensities of the two fragment ions with m/z 259.02 and 241.01 was collision energy dependent, both fragments were always observed simultaneously, contrary to a typical fragmentation pattern of phosphatidylinositol species, in which m/z 241.0 fragment was most abundant.[35]

We further investigated if the fragmentation of IPC species could yield abundant ions that were specific to their ceramide backbone. To this end, we acquired MS^n spectra from their molecular anions on a hybrid linear ion trap–orbitrap mass spectrometer.[28] Orbitrap is a novel Fourier transform orbital trapping mass analyzer.[37,38] To acquire MS^n spectra with high mass accuracy, precursor ions were isolated and fragmented in the linear trap, and spectra were acquired using either the orbitrap analyzer (for higher mass accuracy) or the linear ion trap detector (for better sensitivity). In contrast to instruments equipped with a linear collision cell, such as QqTOF or triple quadrupole mass spectrometers, the collision-induced dissociation of precursor ions in an ion trap usually leaves fragment ions intact, since they fall off the excitation resonance frequency. Therefore, labile intermediate products could be identified and the entire sequence of fragmentation events established via successive fragmentation by MS^n.[25,39] Continuous nanoflow infusion of lipid extracts offered ample time to acquire MS^n spectra with reliable ion statistics. Better

than 30 000 (FWHM) mass resolution, together with better than 3 ppm mass accuracy, achieved by the orbitrap analyzer, allowed us to unequivocally determine the elemental composition of detected fragment ions.

Orbitrap MS^2 analysis of the abundant IPC 44:0;4 species with m/z 952.6897 yielded intense ceramide phosphate fragments $[CerP - H_2O]^-$ and $[CerP]^-$ with m/z 772.6205 and 790.6312, respectively (Fig. 2(B)). The identification of fragment ions was supported by their accurately determined m/z that deviated by less than 3 ppm from the corresponding calculated values, as well as by further MS^3 analysis (see below). In general, similar patterns of fragment ions were observed in MS^2 spectra, acquired from the same precursors on the linear ion trap and on the orbitrap (data not shown). MS^2 spectra did not reveal the exact chemical structure of both ceramide-specific fragments. It was unclear if the loss of H_2O yielded a cyclic phosphate moiety or a double bond elsewhere within the long chain base part of the ceramide backbone. For clarity, we present the structure of (dehydro)ceramide phosphate fragment ions, with a cyclic phosphate moiety between the hydroxyl groups at positions 1 and 3 of the long chain base (Fig. 2(D)); however, alternative isomeric molecular structures are also possible.

Further orbitrap MS^3 analysis of m/z 772.6205 ($[CerP - H_2O]^-$) elucidated the composition of its ceramide backbone (Fig. 2(C)). The fragmentation produced an acyl anion of the fatty acid moiety $[FA26:0;1 + O]^-$ with m/z 411.3840 (mass accuracy 0.7 ppm). Another fragment ion related to the fatty acid moiety was detected at m/z 365.3787 and was produced via subsequent loss of CH_2O, i.e. $[FA26:0;1 - CH_2O]^-$ (mass accuracy 0.6 ppm). These fragments were previously detected in tandem mass spectra of ceramides acquired in negative ion mode on a triple quadrupole instrument.[40,41] Fragments with m/z 378.2412, 363.2305, and 360.2314 were produced via neutral loss of the amide-linked fatty acid, yielding the long chain base phosphate fragment ions $[LCBP18:0;3 - H_2O]^-$ (mass accuracy 0.5 ppm), $[LCBP18:0;3 - H_3NO]^-$ (mass accuracy 0.1 ppm), and $[LCBP18:0;3 - 2H_2O]^-$ (mass accuracy 1.4 ppm), respectively (Fig. 2(C,D)). The fragment ion with m/z 406.2358 was produced by internal cleavage of the fatty acid moiety, resulting in neutral loss of the hydrocarbon chain with secondary α-hydroxyl group ($[LCBP18:0;3 - H_2O + CO]^-$ (mass accuracy 1.5 ppm).

Although we could only speculate on the exact chemical structure of these fragment ions, the orbitrap mass accuracy allowed us to unequivocally determine the number of carbon atoms, hydroxyl groups, and double bonds separately in the long chain base and in the amide-linked fatty acid of their ceramide backbone. Once characteristic fragment ions were identified in orbitrap MS^3 spectra, further structural analysis of low abundant IPC species was performed only on the linear ion trap, which improved the sensitivity and reduced the analysis time (data not shown).

Thus, a combination of QqTOF MS/MS and orbitrap MS^2 and MS^3 fragmentation allowed us to elucidate the chemical composition of the head group and both cleavable parts of the ceramide backbone, i.e. the long chain base and the amide-linked fatty acid (Fig. 2(D)). Interestingly,

no fragments were observed in the MS^3 spectrum that pointed to alternative ceramide structures having different numbers of either methylene or hydroxyl groups. This indicated that the precursor ion IPC 44:0;4 at m/z 952.7 contained a ceramide backbone composed of a long chain base with 18 carbon atoms and three hydroxyl groups (phytosphingosine), together with an amide-linked fatty acid moiety with 26 carbon atoms and one hydroxyl group, i.e. IPC $18:0:3/26:0;1$, which agreed well with the previously reported GC–MS identification of amide-linked fatty acids in sphingolipids from wild-type *S. cerevisiae*.[17]

To further substantiate the structural assignment of fragment ions, we performed orbitrap MS^2 and MS^3 analysis of IPC species isolated from the *elo3Δ* mutant[17]. This mutant lacks the enzymatic activity for elongating fatty acid moieties to C26, and, therefore, mostly synthesises IPC species with C22 amide-linked fatty acids.[17] Orbitrap analysis of an *elo3Δ* lipid extract detected the abundant ion with m/z 896.6260 corresponding to IPC 40:0;4 (data not shown). As expected, its orbitrap MS^2 fragmentation yielded an intense fragment with m/z 716.5590, corresponding to $[CerP - H_2O]^-$ (mass accuracy 1.4 ppm). Further orbitrap MS^3 analysis of $[CerP - H_2O]^-$ produced fragments with m/z 406.2365, 378.2409, 363.2303, and 360.2310, corresponding to the long chain base phosphate fragment ions $[LCBP18:0;3 - H_2O + CO]^-$ (mass accuracy 0.2 ppm); $[LCBP18:0;3 - H_2O]^-$ (mass accuracy 1.3 ppm); $[LCBP18:0;3 - H_3NO]^-$ (mass accuracy 0.6 ppm) and $[LCBP18:0;3 - 2H_2O]^-$ (mass accuracy 0.3 ppm), respectively (data not shown). Exactly the same fragment ions were detected upon orbitrap MS^3 of IPC 18:0;3/26:0;1 isolated from wild-type *S. cerevisiae* (Fig. 2(D)). However, the fragment ion with m/z 355.3220 corresponding to an acyl anion of the fatty acid moiety $[FA22:0;1 + O]^-$ (accuracy 0.6 ppm) was detected in the corresponding MS^3 spectrum of $[CerP - H_2O]^-$ from *elo3Δ* mutant (data not shown). Thus, the comparison of orbitrap MS^2 and MS^3 spectra acquired from IPC 18:0;3/26:0;1 (isolated from wild type) and IPC 18:0;3/22:0;1 (isolated from the *elo3Δ* mutant) species validated the chemical structure of major fragment ions, produced from IPC species comprising phytosphingosine long chain base and different amide-linked fatty acids with α-hydroxyl groups.

We then set out to determine how hydroxyl groups in the long chain base and amide-linked fatty acid moieties affected the fragmentation pathways of IPC species. Two enzyme activities in *S. cerevisiae*, encoded by *scs7* and *sur2* genes, are responsible for the hydroxylation of the ceramide backbone. Scs7p is required for the α-hydroxylation of amide-linked fatty acid moieties[42] (Fig. 1). Sphingolipids, synthesized by the *scs7Δ* mutant, comprise phytosphingosine and an amide-linked fatty acid without an α-hydroxyl group. Sur2p is responsible for converting dihydrosphingosine to phytosphingosine, whereby a hydroxyl group is placed at position 4 of the long chain base[42] (Fig. 1). Thus, the ceramide backbone of sphingolipids from the *sur2Δ* mutant consists of dihydrosphingosine and an amide-linked fatty acid with or without the α-hydroxyl group. The double mutant *sur2Δscs7Δ* is viable and synthesizes sphingolipids
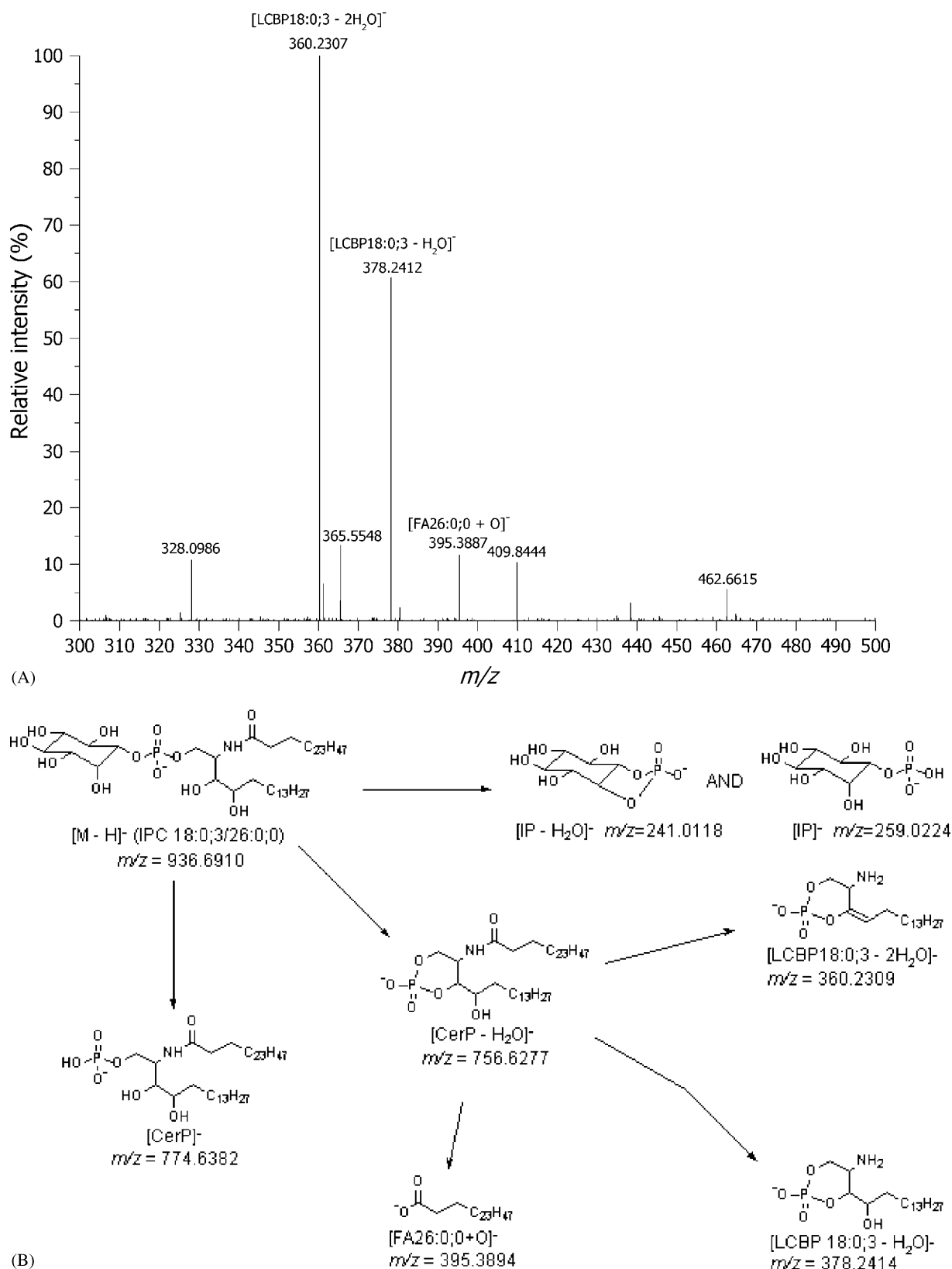
Figure 3. Fragmentation pathways of IPC 18:0;3/26:0;0 isolated from *scs7*Δ mutant. (A) Orbitrap MS³ analysis of intermediate [CerP – H₂O]⁻ fragment (*m/z* 756.6), which was obtained from the molecular anion of IPC 44:0;3 via its MS² fragmentation. Peaks with *m/z* 462.6826, 409.8589, 365.5548, and 328.0986 originate from the background and were not detectable in the ion trap MS³ spectrum from the same precursor (data not shown). (B) Major fragmentation pathways of IPC 18:0;3/26:0;0 isolated from the *scs7*Δ mutant elucidated by QqTOF MS/MS and LTQ Orbitrap MSⁿ analysis.

JMS

with a ceramide backbone containing dihydrosphingosine and an amide-linked fatty acid without α-hydroxyl group.[42]

Orbitrap MS and TOF MS spectra, acquired from a lipid extract of *scs7Δ* mutant, showed an abundant ion at *m/z* 936.6937, corresponding to IPC 44:0;3 (data not shown). Its orbitrap MS^2 analysis yielded intense ceramide phosphate fragments $[CerP - H_2O]^-$ with *m/z* 756.6262 (mass accuracy 2.0 ppm) and $[CerP]^-$ *m/z* 774.6369 (mass accuracy 1.7 ppm) (data not shown). In turn, MS^3 fragmentation of $[CerP - H_2O]^-$ produced two long chain base phosphate fragment ions with *m/z* 378.2412 and 360.2307, corresponding to $[LCBP18:0;3 - H_2O]^-$ (mass accuracy 0.1 ppm) and $[LCBP18:0;3 - 2H_2O]^-$ (mass accuracy 0.6 ppm), respectively (Fig. 3(A,B)). Acyl anion of the amide-linked fatty acid $[FA26:0;0 + O]^-$ was detected at *m/z* 395.3887 (mass accuracy 1.8 ppm) (Fig. 3(A,B)). Wild-type IPC 44:0;4 and IPC 44:0;3 from *scs7Δ* were only different by a single hydroxyl group in the fatty acid backbone (compare Fig. 2(D) with Fig. 3(B)), yet several long chain base-specific fragments were missing in MS^3 spectra of IPC 44:0;3 from *scs7Δ*. Therefore, we speculate that the α-hydroxyl group enhanced the diversity of pathways of neutral loss of fragments of amide-linked fatty acid moieties off the ceramide backbone. Nevertheless, it was possible to unambiguously assign fragments specific for the long chain base and amide-linked fatty acid and thus to identify IPC 44:0;3 from *scs7Δ* mutant as IPC 18:0:3/26:0;0.

We further compared the fragmentation pathways of four IPCs with altered ceramide backbones: IPC 18:0:3/26:0;1 (wild type) (Fig. 2(D)), IPC 18:0:3/26:0;0 (*scs7Δ*) (Fig. 3(B)), IPC 18:0:2/26:0;1 (*sur2Δ*) (data not shown), and IPC 18:0:2/26:0;0 (*sur2Δscs7Δ*) (data not shown). All four IPCs produced a common set of structure-specific fragments. $[LCBP - H_2O]^-$ and $[LCBP - 2H_2O]^-$ were always produced from the long chain base, and the acyl anion $[FA + O]^-$ from the amide-linked fatty acid moiety. If an α-hydroxyl group was present in the amide-linked fatty acid (e.g. IPC 18:0:3/26:0;1, IPC 18:0:2/26:0;1), products of neutral loss of the fatty acid–related fragments $[LCBP - H_2O + CO]^-$ and $[LCBP - H_3NO]^-$ were typically observed, along with another fatty acid–related fragment $[FA - CH_2O]^-$ (Table 1; Figs 2(D), 3(B)). The relative intensities of structure-specific fragment ions varied between IPC species. Fragment ions comprising a long chain base phosphate moiety were, typically, more abundant than fragment ion(s) related to the fatty acid moiety, although the α-hydroxyl group enhanced their intensity.

Thus we concluded that the fragmentation of molecular anions of IPCs on the QqTOF mass spectrometer predominantly produced head group–specific fragments, whereas MS^2 fragmentation on the ion trap yielded abundant ceramide phosphate fragments $[CerP - H_2O]^-$, which served as a starting point for further ceramide backbone-specific fragmentation by MS^3. MS^3 analysis determined the number of carbon atoms, double bonds, and hydroxyl groups in the long chain base and in the amide-linked fatty acid of each fragmented IPC precursor and, hence, enabled their identification as individual molecular species.

Table 1. Structure-specific fragment ions produced from inositol-containing sphingolipids upon MS^3 fragmentation of the abundant $[CerP - H_2O]^-$ fragment ion

| Long chain base moiety	Amide-linked fatty acid moiety	
	With α-hydroxyl group FA X:Y;1[a]	Without α-hydroxyl group FA X:Y;0
Phytos-phingosine LCB X:Y;3[a]	$[LCBP - H_2O]^-$	$[LCBP - H_2O]^-$
	$[LCBP - 2H_2O]^-$	$[LCBP - 2H_2O]^-$
	$[LCB - H_3NO]^-$	$[FA + O]^-$
	$[LCBP - H_2O + CO]^-$	
	$[FA + O]^-$	
	$[FA - CH_2O]^-$	
Dihydro-sphingosine LCB X:Y;2	$[LCBP - H_2O]^-$	$[LCBP - H_2O]^-$
	$[LCBP - 2H_2O]^-$	$[LCBP - 2H_2O]^-$
	$[LCB - H_3NO]^-$	$[FA + O]^-$
	$[LCBP - H_2O + CO]^-$	
	$[FA + O]^-$	
	$[FA - CH_2O]^-$	

[a] X and Y indicate the number of carbon atoms and double bonds in the long chain base or amide-linked fatty acid moiety, respectively.
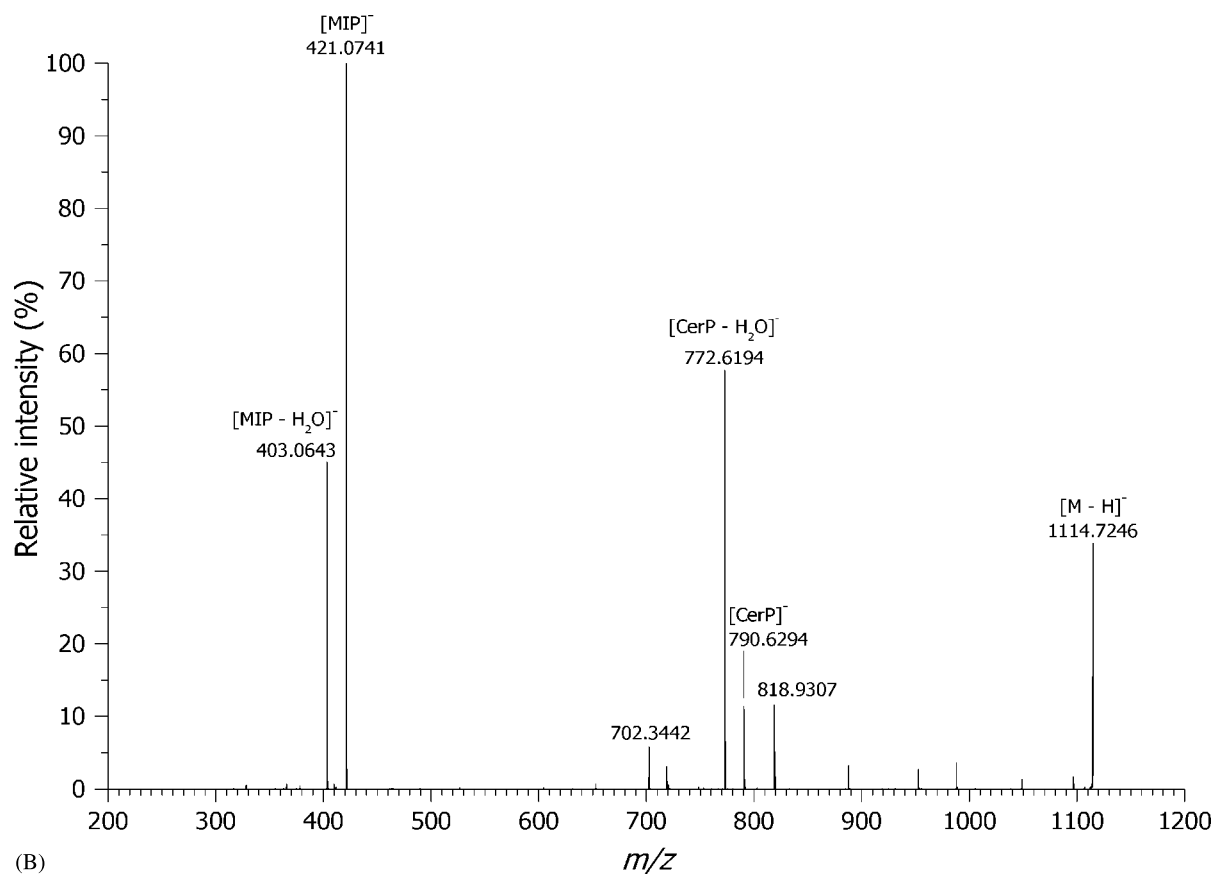
Fragmentation pathways of MIPCs

The most abundant ions in the MIPC fraction were detected on the QqTOF mass spectrometer at *m/z* 1114.74 and 1142.79 and corresponded, respectively, to MIPC 44:0;4 and MIPC 46:0;4 (data not shown), as was also previously observed.[18,34] Tandem mass spectrometry of MIPC species on the QqTOF instrument yielded fragments of the mannosyl-inositolphosphate (MIP) head group: $[MIP]^-$, $[MIP - H_2O]^-$, $[IP]^-$, $[IP - H_2O]^-$, and $[IP - 2H_2O]^-$ (Fig. 4(A,D)). Two fragment ions of very low abundance were detected at *m/z* 790.64 and 772.63, which corresponded to neutral loss of the head group as mannosyl-dehydroinositol ($\Delta m = 324.11$ Da) and produced ceramide phosphate fragments $[CerP]^-$ and $[CerP - H_2O]^-$, respectively. A higher collision energy ($\sim$80 eV) was required for complete dissociation of MIPCs, although the pattern of fragment ions was not altered considerably upon changing the collision energy offset.

Orbitrap MS^2 analysis of MIPC 44:0;4 species demonstrated that fragment ions with *m/z* 790.6294, 772.6194, 421.0741, and 403.0643, were directly produced from the molecular anion (Fig. 4(B,D)). Ion trap MS^3 analysis of $[MIP]^-$ with *m/z* 421.0 produced fragment ions with *m/z* 403.0, 258.8, and 241.1 that corresponded to $[MIP - H_2O]^-$, $[IP]^-$, and $[IP - H_2O]^-$, respectively (Fig. 4(C,D)). Ion trap MS^3 fragmentation of $[MIP - H_2O]^-$ with *m/z* 403.1 produced fragment ions with *m/z* 241.1 and 223.0, corresponding to $[IP - H_2O]^-$ and $[IP - 2H_2O]^-$ (Fig. 4(D), respectively (data not shown).

We concluded that head group ions of MIPCs were fragmented along several parallel pathways. However, at each stage anions of inositol phosphate $[IP]^-$ and dehydroinositol phosphate $[IP - H_2O]^-$ were produced. Yet their abundance was relatively low in the spectra acquired on the QqTOF machine, albeit they were dominating the
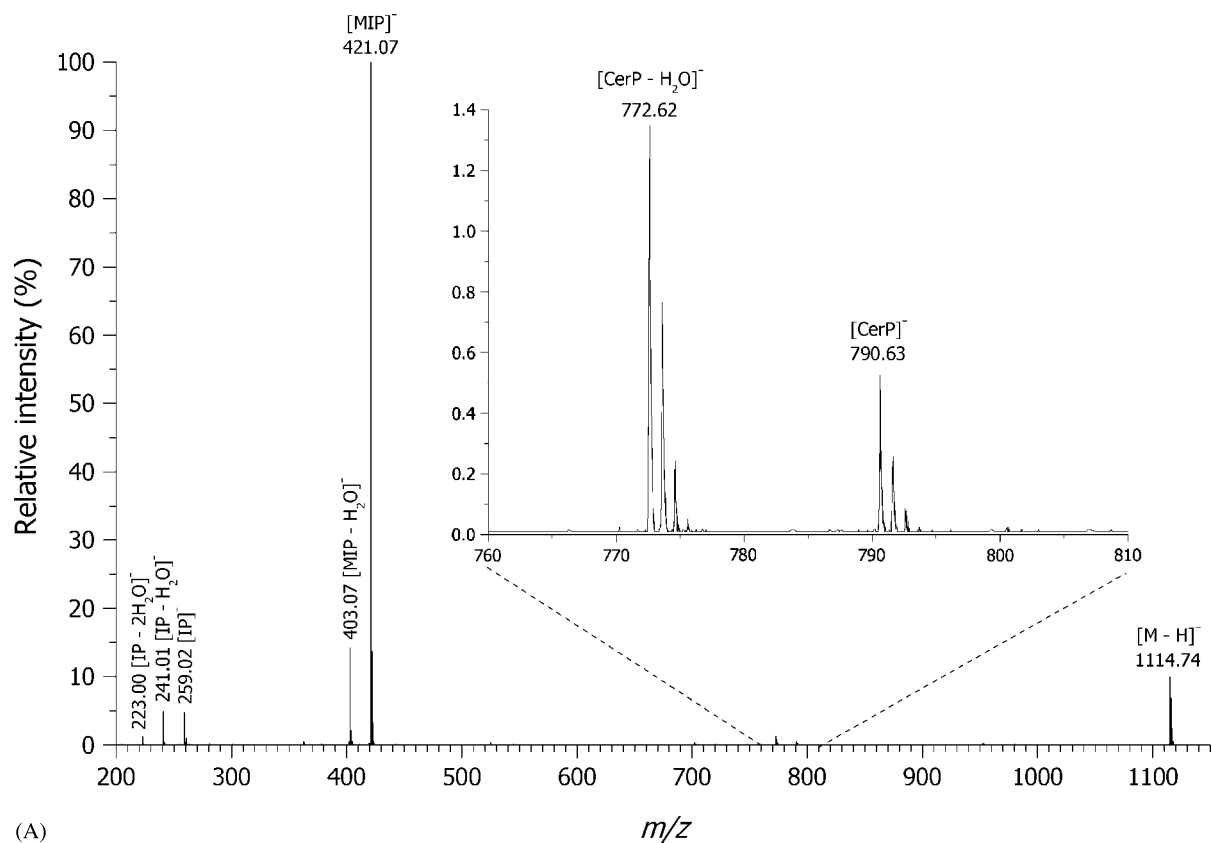
Figure 4. Fragmentation pathways of MIPC species. (A) QqTOF MS/MS spectrum of MIPC 44:0;4 ion of m/z 1114.7 ([M – H]$^-$) acquired at the collision energy of 80 eV. (B) Orbitrap MS^2 spectrum acquired from the same precursor. (C) Ion trap MS^3 spectrum of the head group fragment [MIP]$^-$ with m/z 421.1. (D) Major fragmentation pathways of MIPC 18:0;3/26:0;1 comprising fragments detected in QqTOF MS/MS and LTQ Orbitrap ion MS^n spectra. Note that MS^n fragmentation of m/z 772.6225 [CerP – H$_2$O]$^-$ proceeds according to the same pathways, as presented in Fig. 2(D), and is therefore not shown.
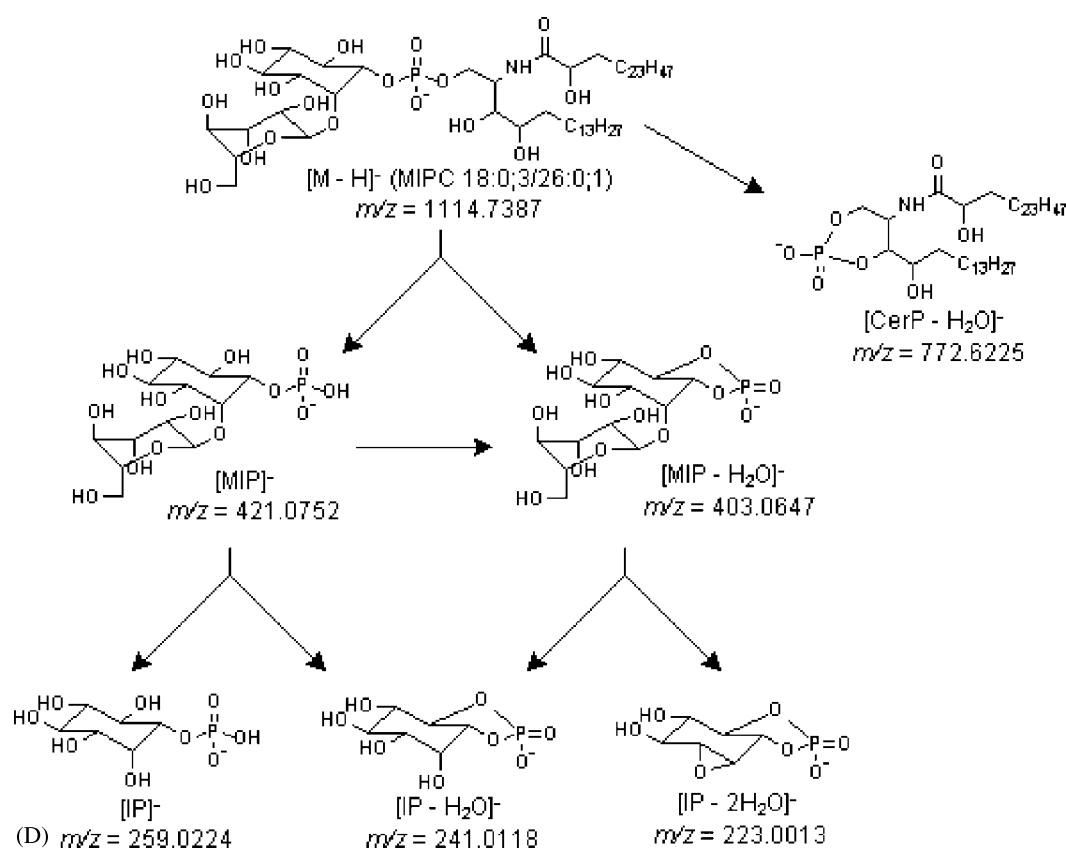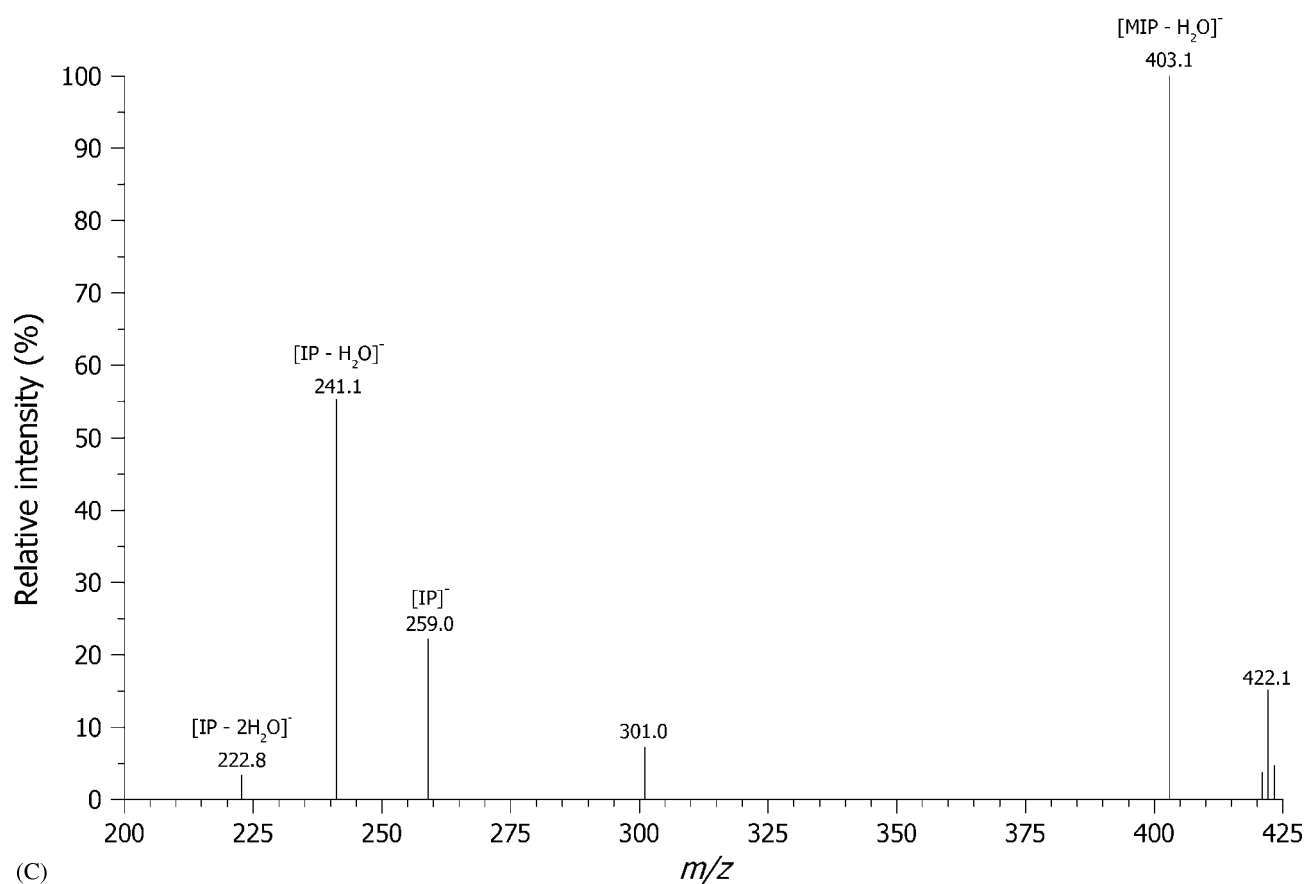
Figure 4. (*Continued*).

spectra of IPCs (Fig. 2(A)). This, presumably, reflected the stability of the glycosidic bond between the inositol and mannose residues in [MIP]$^-$ and [MIP – H$_2$O]$^-$ fragment ions. The fragment ion with m/z 421.07 ([MIP]$^-$) was highly abundant and, since masses of intact IPCs and MIPCs do not overlap, was suitable for class-specific profiling by precursor ion scanning as described below.

Ion trap MS^3 spectrum of [Cer – H$_2$O]$^-$ with m/z 772.6 was similar to MS^3 spectra of the corresponding ceramide fragments of IPC species described above (data not shown). Long chain base phosphate fragment ions were detected at m/z 390.2, 362.3, 347.2, and 344.3 and corresponded to [LCBP18:0;3 – H$_2$O + CO]$^-$, [LCBP18:0;3 – H$_2$O]$^-$, [LCBP 18:0;3 – H$_3$NO]$^-$, and [LCBP18:0;3 – 2H$_2$O]$^-$, respectively. Two fatty acid–related fragment ions were detected at m/z 411.3 and 365.4, corresponding to [FA26:0;1 + O]$^-$ and [FA26:0;1 – CH$_2$O]$^-$, respectively (data not shown). MS^3 analysis of MIPC species from the *sur2Δ* and *scs7Δ* mutants produced similar spectra as obtained for the IPC species from these mutants (data not shown). Thus, MS^3 analysis of the abundant [Cer – H$_2$O]$^-$ fragment elucidated the structure of the ceramide backbone of MIPC species in a similar way, as was demonstrated above for IPC species (Table 1).

Fragmentation pathways of M(IP)$_2$Cs

M(IP)$_2$C species contain two phosphate groups and therefore, in negative ion mode, they were mostly detected as doubly charged ions. Most abundant ions in the M(IP)$_2$C fraction were detected at m/z 677.88 and 691.90 and corresponded to M(IP)$_2$C 44:0;4 and M(IP)$_2$C 46:0;4 (data not shown), as was also observed by Hechtberger *et al*.[18] Tandem mass spectra of M(IP)$_2$C species, acquired on the QqTOF instrument, were dominated by fragments of the mannosyl-diinositolphosphate (M(IP)$_2$) head group: [M(IP)$_2$]$^{2-}$, [M(IP)$_2$ – H$_2$O]$^{2-}$, [M(IP)$_2$ – I]$^{2-}$, [M(IP)$_2$ – P]$^-$, [MIP]$^-$, [MIP – H$_2$O]$^-$, [IP]$^-$, and [IP – H$_2$O]$^-$ (Fig. 5(A)). At the lower collision energy offset, doubly charged mannosyl-diinositolphosphate ([M(IP)$_2$]$^{2-}$) (m/z 331.04) and [M(IP)$_2$ – P]$^-$ (m/z 583.13) were most abundant (Fig. 5(B)), whereas at the higher collision energy offset the fragmentation mainly yielded [IP – H$_2$O]$^-$ (m/z 241.01).

Orbitrap MS^2 and ion trap MS^2 spectra of the M(IP)$_2$C species indicated that [M(IP)$_2$ – P]$^-$, [M(IP)$_2$]$^{2-}$, [M(IP)$_2$ – H$_2$O]$^{2-}$, and [IP – H$_2$O]$^-$ fragments were directly produced from the precursor (Fig. 5(C)) by neutral loss of singly charged head group fragments. The fragment ion with m/z 1114.7316 was produced by cleaving [IP – H$_2$O]$^-$ (m/z 241.0114) fragment off the doubly charged precursor, yielding [M – 2H – 241]$^-$. Loss of the head group as [M(IP)$_2$ – P]$^-$ (m/z 583.1256) and [M(IP)$_2$ – H$_2$O]$^-$ (m/z 645.0815) yielded the ceramide phosphate with m/z 772.6190 ([CerP – H$_2$O]$^-$) and the ceramide with m/z 710.6637 ([Cer]$^-$) fragment ions, respectively (Fig. 5(C,D)).

Further ion trap MS^3 fragmentation of [M(IP)$_2$]$^{2-}$ mainly produced [M(IP)$_2$ – P]$^-$ that subsequently yielded [IP – H$_2$O]$^-$ with m/z 241.0 (data not shown). Hence, [M(IP)$_2$ – P]$^-$ was produced via at least two independent pathways, which eventually rendered [IP – H$_2$O]$^-$ fragment (Fig. 5(D)). MS^3 analysis of the ceramide backbone fragment ion [CerP – H$_2$O]$^-$ with m/z 772.6 produced long chain

base phosphate and fatty acid–related fragments, similar to IPC and MIPC species (data not shown). MS^3 analysis of the [Cer]$^-$ fragment yielded an abundant acyl anion of the amide-linked fatty acid with m/z 411.4 ([FA26:0;1 + O]$^-$) and its neutral loss product with m/z 365.4 ([FA26:0;1 – CH$_2$O]$^-$) (data not shown).

Taken together, we observed strong similarity between the fragmentation pathways of molecular anions of all three classes of inositol-containing sphingolipids and their subtypes. Collision-induced dissociation of precursors on the QqTOF instrument produced fragment ions in which charged phosphate group(s) was (were) attached to the inositol-containing head group, rather than to the ceramide backbone. In QqTOF spectra, ceramide-related fragments were hardly detectable at the collision energy offset required to cleave the precursor ions, although they were abundant in the corresponding ion trap spectra. In the linear collision cell of a QqTOF instrument, multiple-collision fragmentation promoted neutral loss of the ceramide backbone, leaving a net negative charge at the head group. Therefore stable ceramide backbone fragments, such as [FA26:0;1 + O]$^-$, were abundant in ion trap mass spectra; however, they were hardly detectable in spectra acquired on the QqTOF instrument. Importantly, ion trap MS^2 fragmentation of molecular anions of species of all three yeast sphingolipid classes yielded abundant [CerP]$^-$ and [CerP – H$_2$O]$^-$ fragments, paving the way for the characterization of their molecular composition via MS^3 fragmentation. Thus, molecular profiling of sphingolipids was most effectively achieved by combining the complementary mass spectrometric approaches – QqTOF MS/MS lent itself to rapid class-specific profiling, whereas ion trap MS^n enabled the structural elucidation of the ceramide backbone in individual molecular species (Table 1).

Profiling of sphingolipids in yeasts

We used m/z of the abundant fragment ions specific for each sphingolipid class for profiling lipid extracts by the method of multiple precursor ion scanning.[24] The extracts were first subjected to mild alkaline hydrolysis, which destroyed glycerophospholipids. Within each sphingolipid class of *S. cerevisiae*, we detected several species that differed by the total number of carbon atoms and hydroxyl groups in their ceramide backbone (Table 2). The ceramide backbone of the most abundant species of IPCs, MIPCs, and M(IP)$_2$Cs comprised 44 or 46 carbon atoms and four hydroxyl groups, which agreed well with previous observations.[18,34,36] Since M(IP)$_2$C species were detected as doubly charged ions, unit mass resolution of the analytical quadrupole was insufficient to fully resolve their isotopic peaks. However, their identification was further supported by the exact m/z of doubly charged precursor ions, which were easy to recognize in high-resolution TOF MS spectra.

Since inositol-containing sphingolipids commonly occur in various fungi and plants,[43,44] we further tested if their compositional difference could be characterized by multiple precursor ion scanning in several fungi species. In the fission yeast *S. pombe* and the methylotrophic yeast *P. pastoris* both IPC and MIPC species were detectable, whereas M(IP)$_2$C
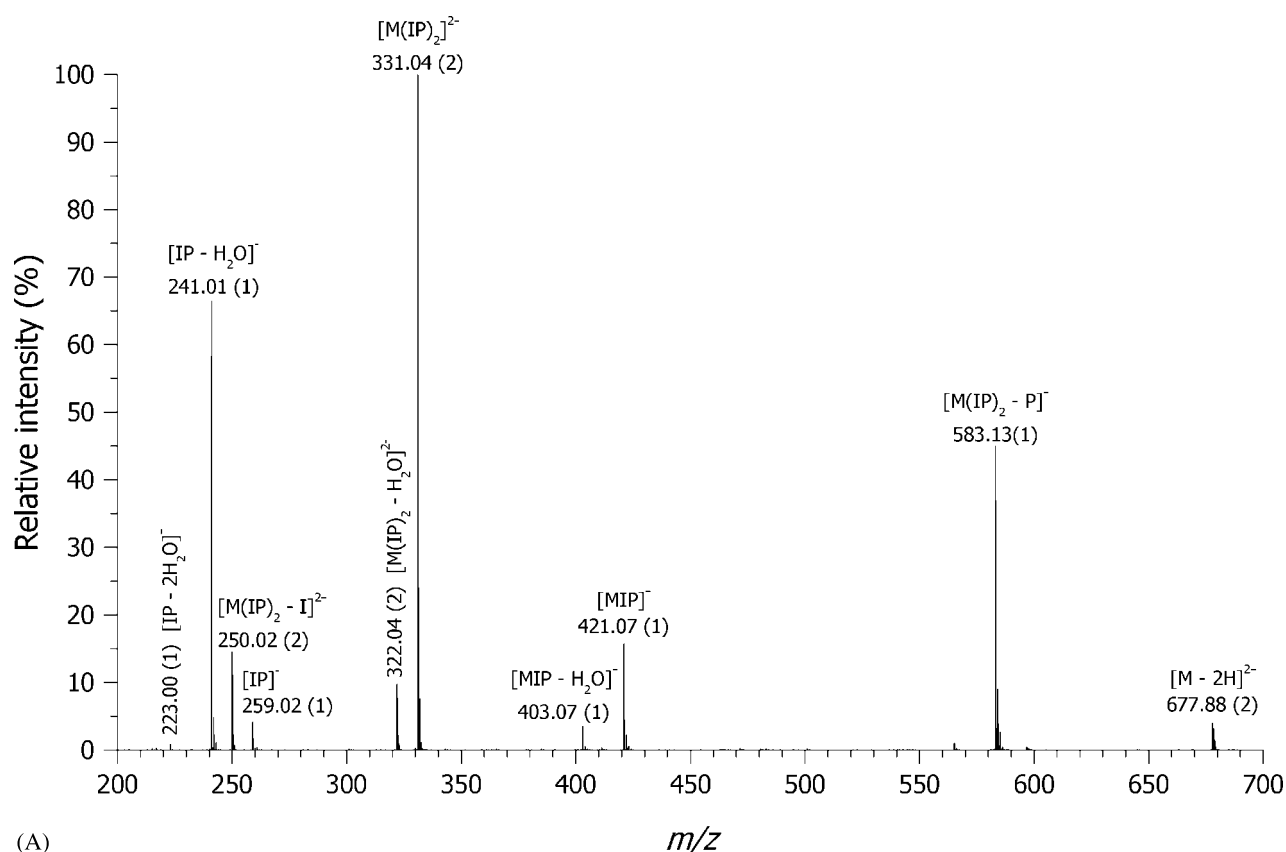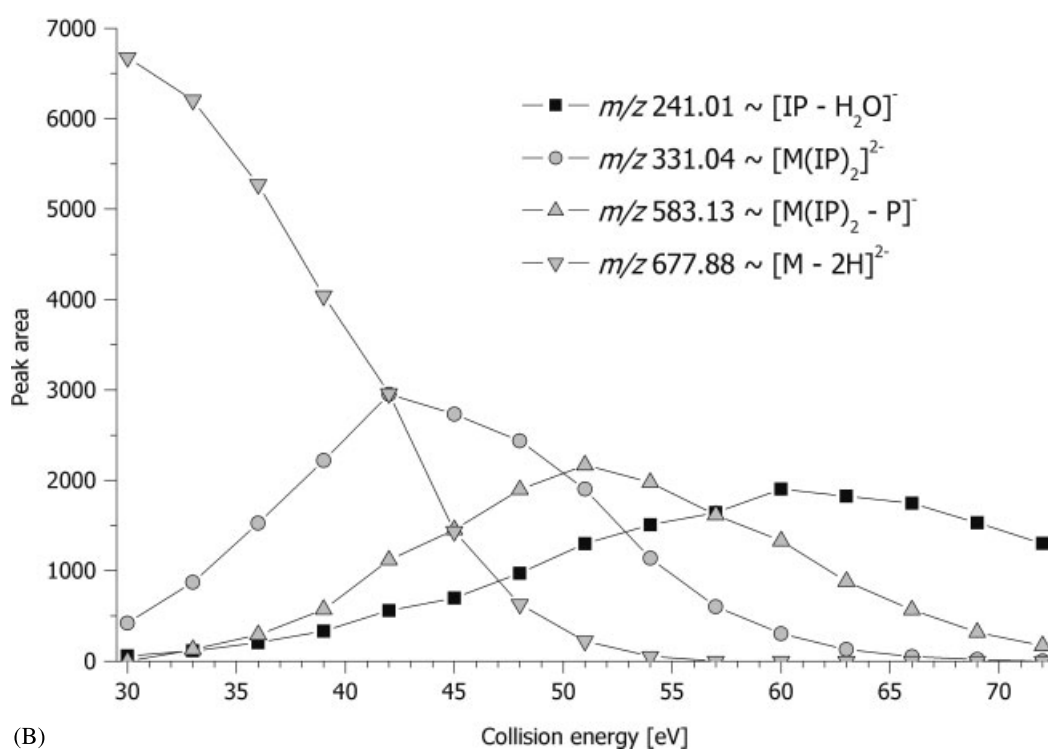
Figure 5. Fragmentation pathways of M(IP)$_2$C species. (A) QqTOF MS/MS spectrum of M(IP)$_2$C 44:0;4 ion having *m/z* 677.9 ([M − 2H]$^{2-}$) acquired at the collision energy of 52 eV. The charges of ions are indicated in brackets. (B) The intensity of fragment ions yielded from the M(IP)$_2$C 44:0;4 species ([M − 2H]$^{2-}$) plotted against the collision energy offset. (C) Orbitrap MS^3 spectrum of M(IP)$_2$C 44:0;4 species ([M − 2H]$^{2-}$) with *m/z* 677.8781. (D) Major fragmentation pathways of M(IP)$_2$C species based on the fragments identified by QqTOF MS/MS and LTQ Orbitrap MS^n. MS^3 fragmentation of *m/z* 772.6225 [CerP − H$_2$O]$^-$ produced the same set of fragments as shown in Fig. 2(D). MS^3 fragmentation of [Cer]$^-$ yielded two fatty acid–specific fragment ions [FA26:0;1 + O]$^-$ and [FA26:0;1 − CH$_2$O]$^-$ (data not shown).
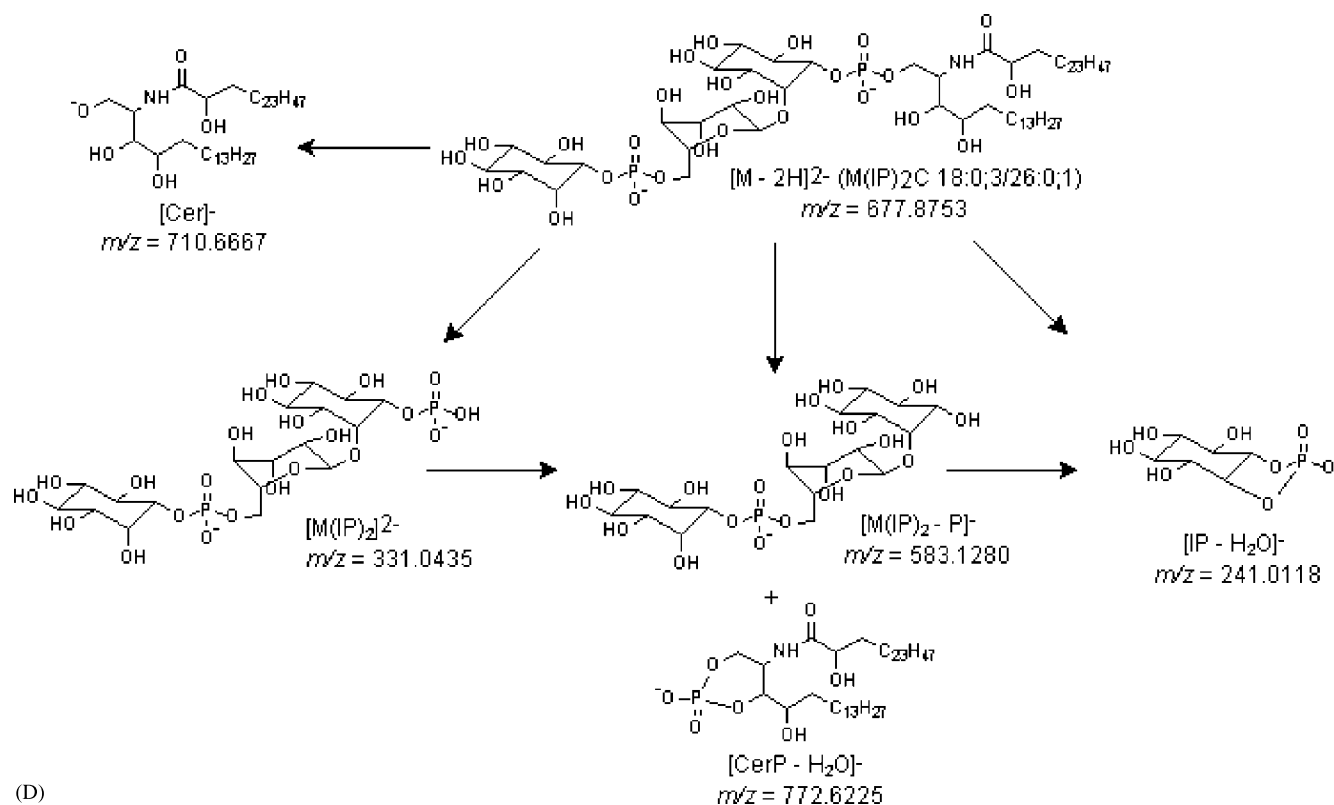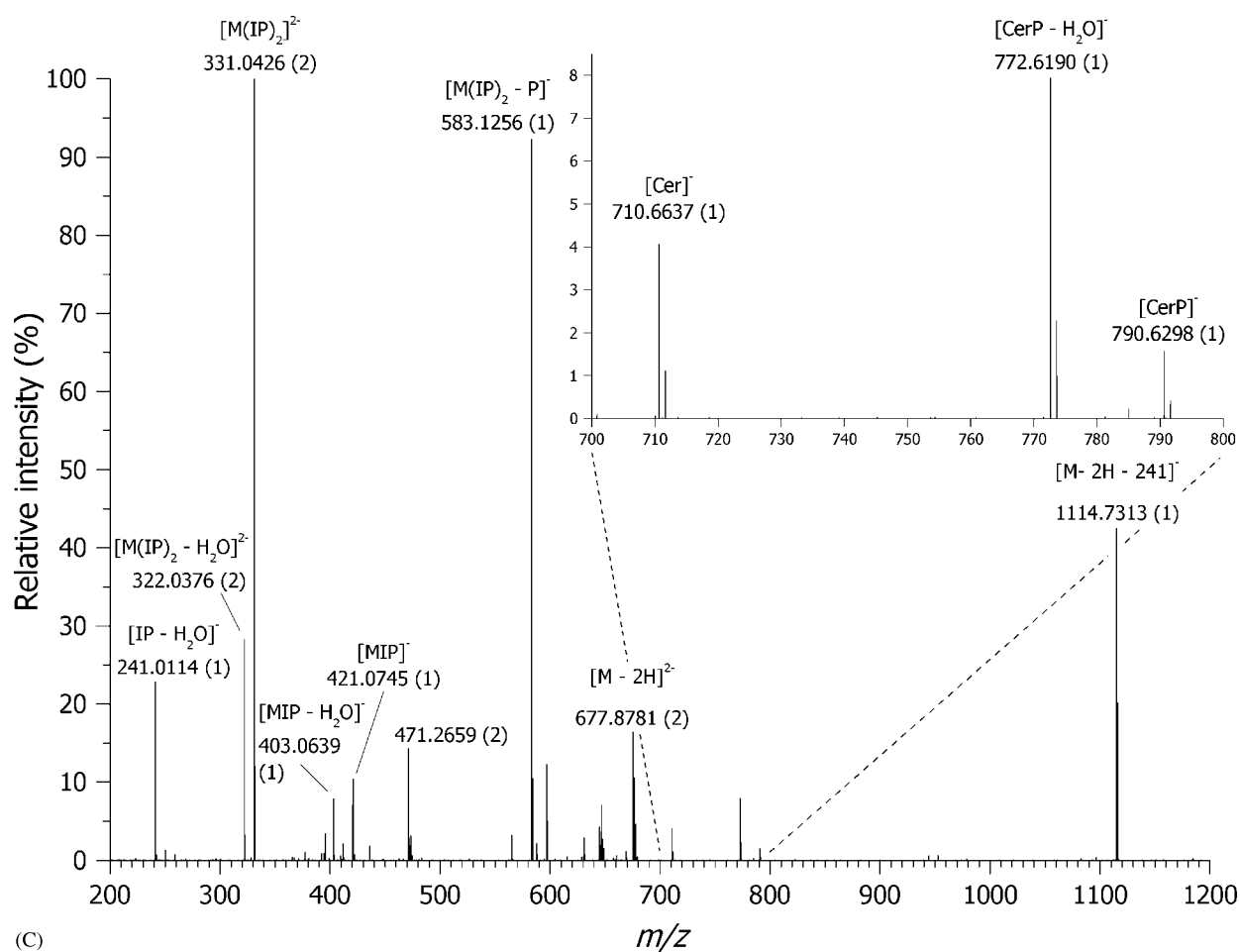
(C)

(D)

Figure 5. (*Continued*).

Table 2. Detection of inositol-containing sphingolipids in various yeasts[a]

IPC species			MIPC species			M(IP)₂C species		
Precursor ion (m/z)	Sum formula	Relative intensity[b] (%)	Precursor ion (m/z)	Sum formula	Relative intensity (%)	Precursor ion[c] (m/z)	Sum formula	Relative intensity (%)
S. cerevisiae								
924.7	42:0;4	11	1098.6	44:0;3	10	655.9	42:0;3	1
936.8	44:0;3	5	1114.6	44:0;4	100	661.9	44:0;2	3
952.7	44:0;4	100	1126.6	46:0;3	4	663.9	42:0;4	2
964.7	46:0;3	4	1130.6	44:0;5	8	669.9	44:0;3	14
968.7	44:0;5	38	1142.6	46:0;4	80	677.9	44:0;4	91
980.7	46:0;4	63	–	–	–	683.9	46:0;3	11
–	–	–	–	–	–	691.9	46:0;4	100
S. pombe								
952.7	44:0;4	100	1114.6	44:0;4	100	Not detected		
968.6	44:0;5	18	1130.6	44:0;5	3			
P. pastoris								
806.5	36:1;2	18	1058.6	40:0;4	3	655.9	42:0;3	12
808.5	36:0;2	24	1070.5	42:0;3	4	663.9	42:0;4	100
810.6	34:1;4	10	1072.6	40:1;5	4	671.9	42:0;5	13
822.6	36:1;3	32	1086.6	42:0;4	100	677.9	44:0;4	24
824.6	36:0;3	17	1100.6	42:1;5	11	685.9	44:0;5	4
908.7	42:0;3	26	1102.5	42:0;5	28	691.9	46:0;4	2
924.7	42:0;4	100	1114.6	44:0;4	27	–	–	–
936.7	44:0;3	10	1128.6	44:1;5	2	–	–	–
938.7	42:1;5	10	1130.5	44:0;5	7	–	–	–
940.5	42:0;5	56	1142.5	46:0;4	2	–	–	–
952.7	44:0;4	52	–	–	–	–	–	–
968.6	44:0;5	11	–	–	–	–	–	–

[a] IPC species were detected by precursor ion scanning for the fragments having m/z 241.0 ([IP – H₂O]⁻) and 259.0 ([IP]⁻) at the collision energy offset of 68 eV. MIPC species were detected by precursor ion scanning for the fragments having m/z 403.1 ([MIP – H₂O]⁻) and 421.1 ([MIP]⁻) at 80 eV. M(IP)₂C species were detected by precursor ion scanning for the fragment ion having m/z 241.0 ([IP – H₂O]⁻), 331.0 ([M(IP)₂]²⁻), and 583.1 ([M(IP)₂ – P]⁻) at the collision energy of 50 eV. All precursor ion scan spectra were acquired in parallel.
[b] Relative intensity within each sphingolipid class.
[c] Doubly charged ions ($z = -2$).

species were only identified in *P. pastoris* (Table 2). A ceramide backbone with 44 carbon atoms and 4 hydroxyl groups was typical for IPC and MIPC species in *S. pombe*. A previous study identified C20 phytosphingosine as the most common type of a long chain base in *S. pombe*.[15] Therefore the most abundant IPC and MIPC species of *S. pombe* probably comprise an amide-linked monohydroxylated C24 fatty acid moiety (e.g. producing IPC 20:0;3/24:0;1). It was also reported that *S. pombe* synthesizes sphingolipids with monounsaturated C20 sphingosine long chain base;[15] however, no such species were detected among IPC and MIPC species in this work.

The sum formula of inositol-containing sphingolipids in *P. pastoris* strongly varied (Table 2), especially within the IPC class. *P. pastoris* mainly synthesized species with a ceramide backbone of 42 carbon atoms and 4 hydroxyl groups, whereas in *S. cerevisiae* and *S. pombe* species with 44 carbon atoms and 4 hydroxyl groups were the most abundant. Taken together,

rapid and accurate profiling of the sphingolipid composition in several fungi organisms suggested that multiple precursor ion scanning is a valuable tool for elucidating molecular details of sphingolipid biosynthesis.

Simultaneous profiling of sphingolipids and glycerophospholipids

Ion trapping capabilities[33] of a QqTOF mass spectrometer enable the simultaneous acquisition of precursor ion spectra for a large number of fragment ions. We previously demonstrated that multiple precursor ion scanning could rapidly decipher the molecular composition of glycerophospholipid species.[24,25] Upon collision-induced dissociation, molecular anions of glycerophospholipids produced acyl anions of their fatty acid moieties.[35,45–47] If masses of all possible acyl anions were selected for multiple precursor ion scanning, individual lipid species would be detected in the two precursor ion scans, corresponding to their fatty acid moieties.
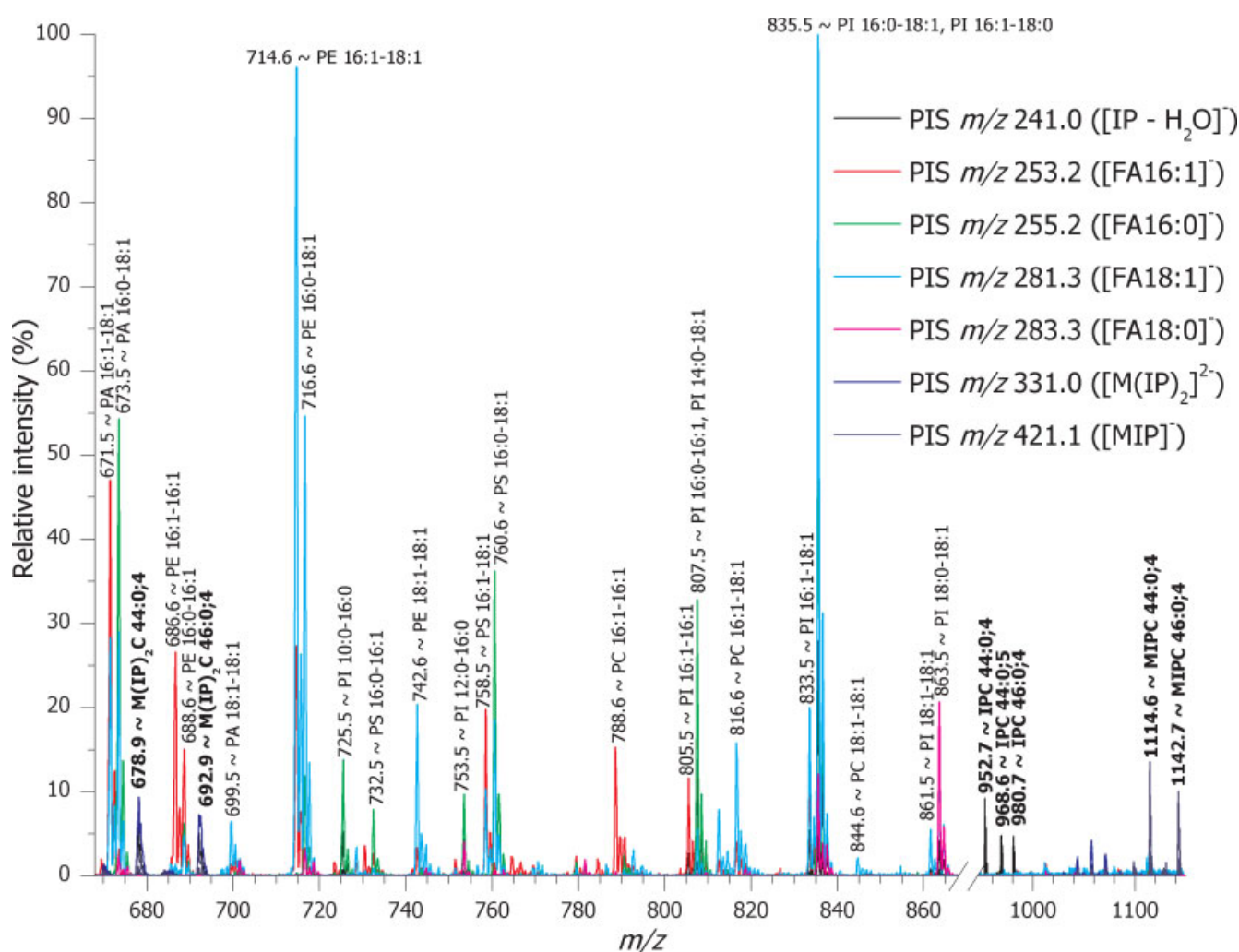
Figure 6. Simultaneous profiling of *S. cerevisiae* sphingolipids and glycerophospholipids from an unseparated lipid extract by multiple precursor ion scanning. Precursor ion spectra for 17 fragment ions corresponding to acyl anions of major fatty acids produced from glycerophospholipid species and 11 fragment ions produced from sphingolipid head groups (for clarity of presentation, only seven scans are presented in the figure). Peaks were identified by prototype *Lipid Profiler* software. Sphingolipids and glycerophospholipids detected are annotated as described in the 'Materials and Methods' section. Sphingolipid species detected are shown in bold.

Since m/z of acyl anions of fatty acids do not overlap with m/z of characteristic fragments of sphingolipids, we reasoned that glycerophospholipids and sphingolipids could be simultaneously and independently detected in crude lipid extracts.

As a case study, we analyzed an unseparated lipid extract from *S. cerevisiae*. The m/z of six acyl anions of the most common saturated and monounsaturated fatty acids, with 14, 16, and 18 carbon atoms, and 11 yeast sphingolipid fragment ions were selected (Fig. 6). Since optimal collision energy depends on the lipid class, we ramped it linearly from 48 eV at m/z 650 to 82 eV at m/z 1150. Seventeen simultaneously acquired precursor ion scan spectra were interpreted by prototype *Lipid Profiler* software[48] and all prominent peaks automatically identified (Fig. 6). Thus, multiple precursor ion scanning enabled simultaneous and specific profiling of IPC, MIPC, and M(IP)$_2$C species, together with the identification of the molecular composition of individual species of phosphatidylinositols, phosphatidic

acids, phosphatidylethanolamines, phosphatidylserines, and phosphatidylcholines. Similar results were obtained on crude lipid extracts of *S. pombe* and *P. pastoris* (data not shown).

CONCLUSIONS

We elucidated the fragmentation pathways of inositol-containing sphingolipids that are synthesized by plants and fungi. Upon collision-induced dissociation of their molecular anions on a QqTOF instrument, sphingolipids produced class-specific fragment ions, originating from their inositol-containing head groups. We further demonstrated that, by accounting for the number of carbon atoms, double bonds, and hydroxyl groups at the corresponding amide-linked fatty acid and the long chain base, ion trap MS^2 and MS^3 fragmentation provided important details on the structure of the ceramide backbone of sphingolipids. By comparing MS^3 spectra acquired from the [CerP – H$_2$O]$^-$ fragment obtained from IPC species with different ceramide

backbones, we demonstrated that all inositol-containing sphingolipid species yielded a common set of major fragment ions. Their unequivocal structural assignment was achieved by acquiring spectra on the LTQ Orbitrap machine with better than 3 ppm mass accuracy. The α-hydroxyl group in amide-linked fatty acid moieties enhanced ceramide fragmentation and produced additional fragments specific for their long chain bases (Table 1). The m/z of sphingolipid fragment ions, rendered from their head groups, did not overlap with the m/z of acyl anions of common fatty acids, which enabled simultaneous profiling of sphingolipids and glycerophospholipids in total lipid extracts. As a case study, we compared the sphingolipid profiles in the yeasts *S. cerevisiae*, *S. pombe*, and *P. pastoris*, which revealed that the composition of their ceramide backbones was remarkably diverse. Upon further automation by auto-sampling,[49,50] automated data−dependent lipid profiling,[51] peak annotation, and data analysis,[48] the approach lent itself to a variety of screening applications, including the molecular analysis of mutant phenotypes and the effect of growth conditions and drugs on sphingolipid metabolism in a variety of model organisms.[43,44]

Acknowledgements

REFERENCES

1. Funato K, Vallee B, Riezman H. Biosynthesis and trafficking of sphingolipids in the yeast *Saccharomyces cerevisiae*. *Biochemistry* 2002; **41**: 15105.
2. Boumann HA, Damen MJA, Versluis C, Heck AJR, de Kruijff B, de Kroon A. The two biosynthetic routes leading to phosphatidylcholine in yeast produce different sets of molecular species. Evidence for lipid remodeling. *Biochemistry* 2003; **42**: 3054.
3. Boumann HA, de Kruijff B, Heck AJ, de Kroon AI. The selective utilization of substrates in vivo by the phosphatidylethanolamine and phosphatidylcholine biosynthetic enzymes Ept1p and Cpt1p in yeast. *FEBS Lett.* 2004; **569**: 173.
4. Natter K, Leitner P, Faschinger A, Wolinski H, McCraith S, Fields S, Kohlwein SD. The spatial organization of lipid synthesis in the yeast saccharomyces cerevisiae derived from large scale green fluorescent protein tagging and high resolution microscopy. *Mol. Cell. Proteomics* 2005; **4**: 662.
5. Schneiter R, Brugger B, Sandhoff R, Zellnig G, Leber A, Lampl M, Athenstaedt K, Hrastnik C, Eder S, Daum G, Paltauf F, Wieland FT, Kohlwein SD. Electrospray ionization tandem mass spectrometry (ESI-MS/MS) analysis of the lipid molecular species composition of yeast subcellular membranes reveals acyl chain-based sorting/remodeling of distinct molecular species en route to the plasma membrane. *J. Cell Biol.* 1999; **146**: 741.
6. Schneiter R. Brave little yeast, please guide us to Thebes: sphingolipid function in *S. cerevisiae*. *BioEssays* 1999; **21**: 1004.
7. Dickson RC, Lester RL. Sphingolipid functions in *Saccharomyces cerevisiae*. *Biochim. Biophys. Acta* 2002; **1583**: 13.
8. Bagnat M, Chang A, Simons K. Plasma membrane proton ATPase Pma1p requires raft association for surface delivery in yeast. *Mol. Biol. Cell* 2001; **12**: 4129.
9. Bagnat M, Keranen S, Shevchenko A, Simons K. Lipid rafts function in biosynthetic delivery of proteins to the cell surface in yeast. *Proc. Natl. Acad. Sci. USA* 2000; **97**: 3254.
10. Bagnat M, Simons K. Cell surface polarization during yeast mating. *Proc. Natl. Acad. Sci. USA* 2002; **99**: 14183.
11. Eisenkolb M, Zenzmaier C, Leitner E, Schneiter R. A specific structural requirement for ergosterol in long-chain fatty acid synthesis mutants important for maintaining raft domains in yeast. *Mol. Biol. Cell* 2002; **13**: 4414.
12. Dickson RC, Lester RL. Metabolism and selected functions of sphingolipids in the yeast *Saccharomyces cerevisiae*. *Biochim. Biophys. Acta* 1999; **1438**: 305.
13. Sims KJ, Spassieva SD, Voit EO, Obeid LM. Yeast sphingolipid metabolism: clues and connections. *Biochem. Cell Biol.* 2004; **82**: 45.
14. Patton JL, Lester RL. The phosphoinositol sphingolipids of *Saccharomyces cerevisiae* are highly localized in the plasma membrane. *J. Bacteriol.* 1991; **173**: 3101.
15. Garton S, Michaelson LV, Beaudoin F, Beale MH, Napier JA. The dihydroceramide desaturase is not essential for cell viability in *Schizosaccharomyces pombe*. *FEBS Lett.* 2003; **538**: 192.
16. Smith SW, Lester RL. Inositol phosphorylceramide, a novel substance and the chief member of a major group of yeast sphingolipids containing a single inositol phosphate. *J. Biol. Chem.* 1974; **249**: 3395.
17. Oh CS, Toke DA, Mandala S, Martin CE. ELO2 and ELO3, homologues of the Saccharomyces cerevisiae ELO1 gene, function in fatty acid elongation and are required for sphingolipid formation. *J. Biol. Chem.* 1997; **272**: 17376.
18. Hechtberger P, Zinser E, Saf R, Hummel K, Paltauf F, Daum G. Characterization, quantification and subcellular localization of inositol-containing sphingolipids of the yeast Saccharomyces cerevisiae. *Eur. J. Biochem.* 1994; **225**: 641.
19. Han X, Gross RW. Electrospray ionization mass spectroscopic analysis of human erythrocyte plasma membrane phospholipids. *Proc. Natl. Acad. Sci. USA* 1994; **91**: 10635.
20. Han XL, Gross RW. Structural determination of picomole amounts of phospholipids via electrospray ionization tandem mass spectrometry. *J. Am. Soc. Mass Spectrom.* 1995; **6**: 1202.
21. Kerwin JL, Tuininga AR, Ericsson LH. Identification of molecular species of glycerophospholipids and sphingomyelin using electrospray mass spectrometry. *J. Lipid Res.* 1994; **35**: 1102.
22. Taguchi R, Hayakawa J, Takeuchi Y, Ishida M. Two-dimensional analysis of phospholipids by capillary liquid chromatography/electrospray ionization mass spectrometry. *J. Mass Spectrom.* 2000; **35**: 953.
23. Brugger B, Erben G, Sandhoff R, Wieland FT, Lehmann WD. Quantitative analysis of biological membrane lipids at the low picomole level by nanoelectrospray ionization tandem mass spectrometry. *Proc. Natl. Acad. Sci. USA* 1997; **94**: 2339.
24. Ekroos K, Chernushevich IV, Simons K, Shevchenko A. Quantitative profiling of phospholipids by multiple precursor ion scanning on a hybrid quadrupole time-of-flight mass spectrometer. *Anal. Chem.* 2002; **74**: 941.
25. Ekroos K, Ejsing CS, Bahr U, Karas M, Simons K, Shevchenko A. Charting molecular composition of phosphatidylcholines by fatty acid scanning and ion trap MS3 fragmentation. *J. Lipid Res.* 2003; **44**: 2181.
26. Chernushevich I, Loboda A, Thomson B. An introduction to quadrupole time-of-flight mass spectrometry. *J. Mass Spectrom.* 2001; **36**: 849.
27. Olsen JV, de Godoy LM, Li G, Macek B, Mortensen P, Pesch R, Makarov A, Lange O, Horning S, Mann M. Parts per million mass accuracy on an orbitrap mass spectrometer via lock-mass injection into a C-trap. *Mol. Cell. Proteomics* 2005; **4**: 2010.

28. Hu QZ, Noll RJ, Li HY, Makarov A, Hardman M, Cooks RG. The Orbitrap: a new mass spectrometer. *J. Mass Spectrom.* 2005; **40**: 430.

29. Sherman F. Getting started with yeast. *Methods Enzymol.* 1991; **194**: 3.

30. Serrano R. H +-ATPase from plasma membranes of *Saccharomyces cerevisiae* and *Avena sativa* roots – purification and reconstitution. *Methods Enzymol.* 1988; **157**: 533.

31. Hechtberger P, Daum G. Intracellular-transport of inositol-containing sphingolipids in the yeast *Saccharomyces cerevisiae*. *FEBS Lett.* 1995; **367**: 201.

32. Ekroos K, Shevchenko A. Simple two-point calibration of hybrid quadrupole time-of-flight instruments using a synthetic lipid standard. *Rapid Commun. Mass Spectrom.* 2002; **16**: 1254.

33. Chernushevich I. Duty cycle improvement for a quadrupole time-of-flight mass spectrometer and its use for precursor ion scans. *Eur. J. Mass Spectrom.* 2000; **6**: 471.

34. Gaigg B, Neergaard TBF, Schneiter R, Hansen JK, Faergeman NJ, Jensen NA, Andersen JR, Friis J, Sandhoff R, Schroder HD, Knudsen J. Depletion of acyl-coenzyme a-binding protein affects sphingolipid synthesis and causes vesicle accumulation and membrane defects in *Saccharomyces cerevisiae*. *Mol. Biol. Cell* 2001; **12**: 1147.

35. Hsu FF, Turk J. Characterization of phosphatidylinositol, phosphatidylinositol-4- phosphate, and phosphatidylinositol-4,5-bisphosphate by electrospray ionization tandem mass spectrometry: a mechanistic study. *J. Am. Soc. Mass Spectrom.* 2000; **11**: 986.

36. Young ME, Karpova TS, Brugger B, Moschenross DM, Wang GK, Schneiter R, Wieland FT, Cooper JA. The Sur7p family defines novel cortical domains in *Saccharomyces cerevisiae*, affects sphingolipid metabolism, and is involved in sporulation. *Mol. Cell. Biol.* 2002; **22**: 927.

37. Makarov A. Electrostatic axially harmonic orbital trapping: a high-performance technique of mass analysis. *Anal. Chem.* 2000; **72**: 1156.

38. Hardman M, Makarov AA. Interfacing the orbitrap mass analyzer to an electrospray ion source. *Anal. Chem.* 2003; **75**: 1699.

39. Larsen A, Uran S, Jacobsen PB, Skotland T. Collision-induced dissociation of glycero phospholipids using electrospray ion-trap mass spectrometry. *Rapid Commun. Mass Spectrom.* 2001; **15**: 2393.

40. Han X. Characterization and direct quantitation of ceramide molecular species from lipid extracts of biological samples by electrospray ionization tandem mass spectrometry. *Anal. Biochem.* 2002; **302**: 199.

41. Hsu FF, Turk J. Characterization of ceramides by low energy collisional-activated dissociation tandem mass spectrometry with negative-ion electrospray ionization. *J. Am. Soc. Mass Spectrom.* 2002; **13**: 558.

42. Haak D, Gable K, Beeler T, Dunn T. Hydroxylation of *Saccharomyces cerevisiae* ceramides requires Sur2p and Scs7p. *J. Biol. Chem.* 1997; **272**: 29704.

43. Dickson RC, Lester RL. Yeast sphingolipids. *Biochim. Biophys. Acta* 1999; **1426**: 347.

44. Sperling P, Heinz E. Plant sphingolipids: structural diversity, biosynthesis, first genes and functions. *Biochim. Biophys. Acta* 2003; **1632**: 1.

45. Hsu FF, Turk J. Charge-remote and charge-driven fragmentation processes in diacyl glycerophosphoethanolamine upon low-energy collisional activation: a mechanistic proposal. *J. Am. Soc. Mass Spectrom.* 2000; **11**: 892.

46. Hsu FF, Turk J. Charge-driven fragmentation processes in diacyl glycerophosphatidic acids upon low-energy collisional activation. A mechanistic proposal. *J. Am. Soc. Mass Spectrom.* 2000; **11**: 797.

47. Hsu FF, Turk J. Studies on phosphatidylglycerol with triple quadrupole tandem mass spectrometry with electrospray ionization: fragmentation processes and structural characterization. *J. Am. Soc. Mass Spectrom.* 2001; **12**: 1036.

48. Ejsing CS, Duchoslav E, Simons K, Thiele C, Ekroos K, Shevchenko A. Automated identification and quantification of molecular species of lipids by multiple precursor ion scanning. Submitted.

49. Schultz GA, Corso TN, Prosser SJ, Zhang S. A fully integrated monolithic microchip electrospray device for mass spectrometry. *Anal. Chem.* 2000; **72**: 4058.

50. Zhang S, Van Pelt CK. Chip-based nanoelectrospray mass spectrometry for protein characterization. *Expert Rev. Proteomics* 2004; **1**: 449.

51. Schwudke D, Oegema J, Burton L, Entchev E, Hannich JT, Ejsing CS, Kurzchalia T, Shevchenko A. Lipid profiling by multiple precursor and neutral loss scanning driven by the data dependent acquisition. *Anal. Chem.* 2005; **78**: 585.